BA48395943　　土奇大　　524/M

# 大偏心を有する高性能外ケーブル式ＰＣ構造物の開発及び設計手法の作成

（１０５５５１４７）

平成 10 年度～平成 11 年度科学研究費補助金（基盤研究(B)(2)）研究成果報告書

平成 12 年 3 月

研究代表者　睦好宏史

（埼玉大学工学部教授）

埼大コーナー

埼玉大学附属図書館
998001141

平成10年度～平成11年度科学研究費補助金（基盤研究(B)(2)）研究成果報告書

課題番号：１０５５５１４７

研究課題：大偏心を有する高性能外ケーブル式ＰＣ構造物の開発及び設計手法の作成

研究組織：
研究代表者：睦好宏史（埼玉大学工学部教授）
研究分担者：
（１）牧　剛史（埼玉大学工学部助手）
（２）渡辺宗樹（三井建設（株）土木本部ＰＣ技術部部長代理）
（３）ドーピー建設工業（株）技術センター副主任研究員

研究経費：
平成10年度：3,900千円
平成11年度：2,000千円
計　　：5,900千円

研究発表：

1)Aravinthan, T., Mutsuyoshi, H., Fujioka, A. and Hishiki, Y.:Prediction of the Ultimate Flexural Strength of Externally Prestressed PC Beams, Proceedings of JCI, Vol.19, No.2, 1997( in printing)

2) T. Aravinthan, H. Mutsuyoshi, T. Niitsu and An Chen: Flexural Behavior of Externally Prestressed Beams with Large Eccentricities, Proc. of the Japan Concrete Institute, Vol.20, No.3,pp.673-678, 1998

3) T. Aravinthan, H. Mutsuyoshi and Y. Hishiki : Flexural Strength and Ductility of PC Beams With External Prestressing, The 6th EASEC, Vol.2, pp.805-810, 1998

4) T. Aravinthan, H. Mutsuyoshi and Y. Hishiki : Ultimate Strength and Ductility of PC Beams with External Tendons, IABSE SYMPOSIUM "Long-Span and High-rise Structures", Kobe, Japan pp.191-192, 1998

5) T. Aravinthan, H. Mutsuyoshi, Y. Hamada, M. Watanabe:Experimental Investigation on the Flexural Behavior of Tow Span Continuous Beams with Large Eccentricities, Proc. of the Japan Concrete Institute, Vol.21, No.3, pp.961-966, 1999

6) T. Aravinthan, H. Mutsuyoshi, S. Tamura, M. Watanabe:Behavior of Continuous Beams with External Prestressing Having Large Eccentricities, Proceedings of the Seventh East Asia-Pacific Conference on Structural Engineering & Construction August 27-29, Vol.1, pp.483-494, 1999, Kochi, Japan

7) 篠崎裕生・渡辺宗樹・松井敏二・睦好宏史：大偏心ケーブルトラス PC 連続桁構造の振動・クリープ特性について
8) 田村　聖・T. Aravinthan・三上　浩・睦好宏史：大偏心ケーブルを有する 2 径間連続はりの曲げ性状に関する実験的研究，第９回プレストレスコンクリートの発展に関するシンポジウム論文集，pp.563-568，1999
9) H. MUTSUYOSHI, T. ARAVINTHAN, S. TAMURA, M. WATANABE and H. SHINOZAKI, New PC Truss Bridge Using External Tendons with Large Eccentricity, IABSE Congress, 1999(printing)

# CONTENTS

# LISTS OF FIGURES

# LISTS OF TABLES

# LISTS OF PHOTOGRAPHS

# CHAPTER 1

# Introduction

## 1.1 General

It has been generally known that in recent years the application of external prestressing is becoming more popular and widely used for bridge structures. This type of construction has been indicated that not only a simplicity in construction work but also a substantial reduction of construction time and cost could be achieved especially when applied to the precast segmental construction method.

In this type of prestressing method, a major portion of external tendons is placed outside the concrete section and connected to the structural member at the deviators and anchorages. As a result, there is no bond between external tendons and surrounding concrete and the prestressing force can be transmitted to the concrete structure through only the end anchorages and deviators. This implies that the strain compatibility at any section can no longer be maintained in the analysis of externally prestressed concrete structures. These facts lead to a "*member-dependent*" characteristic of the overall behavior of EPC structure when subjected to external load.

In this chapter, a discussion of the development of external prestressing with large eccentricities is presented along with the definition of this innovative type of structure. In addition, some previous investigations regarding the flexural and shear behavior of externally PC structure are reviewed and, finally, the objectives and scope of present study are described.

### 1.1.1 Development of EPC Structure with Large Eccentricities

Even though the externally PC structure is considered having many advantages, some shortcomings are also encountered. One of those disadvantages which are being much concerned is that the ultimate flexural strength is comparatively lower than that of PC beams with internal bonded tendons. This is especially true for precast box girder beams in which the maximum eccentricities of external tendons are limited at the level of bottom slab, causing a reduction of tendon eccentricity at critical sections (Fig. 1-1).

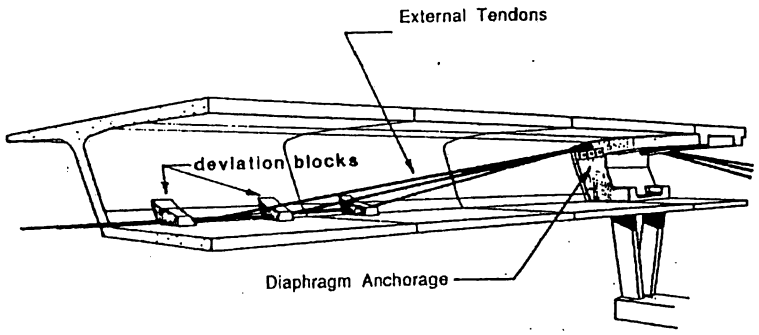


**Fig. 1-1 Limitation of tendon eccentricity in typical box-girder bridge** [1]

Many researches have been carried out indicating that the ultimate flexural strength as well as the ductility of externally PC structure can be improved by the use of a mixed prestressing method comprising external and internal bonded tendon. Another methodology recently proposed by Aravinthan, et al. (1998 [2]) is to increase tendon eccentricity by placing external tendon outside the concrete section at large eccentricities. By using this concept, it has been found that an effective utilization of external tendon as a tension member and concrete section as a compression one could be obtained leading to a substantial enhancement of the ultimate flexural strength. Moreover, this innovative concept of external prestressing was also extended to continuous girders in which a better structural performance considering the serviceability condition could be obtained (Aravinthan, et al., 1999 [3]) This newly developed concept, however, has not yet been applied to precast segmental construction which has been extensively utilized in many bridge structures nowadays. In order to investigate the flexural behavior of such beams, an experimental as well as an analytical program were carried out by taking into account of the effect of casting method and the provision of internal unbonded tendon. Furthermore,

an experimental investigation on shear behavior was also conducted in order to obtain a better understanding of shear behavior in this type of structure.

### 1.1.2 Definition of EPC Structure with Large Eccentricities

External prestressing with large eccentricities can be defined as a prestressing method in which the external tendons are placed considerably outside the depth of concrete structure. From this point of view, its definition is considered to be similar to those of extradosed PC bridge. A difference can be made between these two new concepts by considering that in extradosed PC bridges the external tendons are generally provided at the level beyond the concrete girder by anchored between main tower and anchorages along girder length (Fig.1-2). In EPC beam with large eccentricities, the external tendons are placed continuously throughout the concrete girder length and attached only at the deviators and the end anchorages (Fig.1-3). Therefore, the overall behavior of this kind of structure will be similar to that of ordinary PC beams with external tendon rather than a cable-stayed bridge as is the case for extradosed PC bridge.

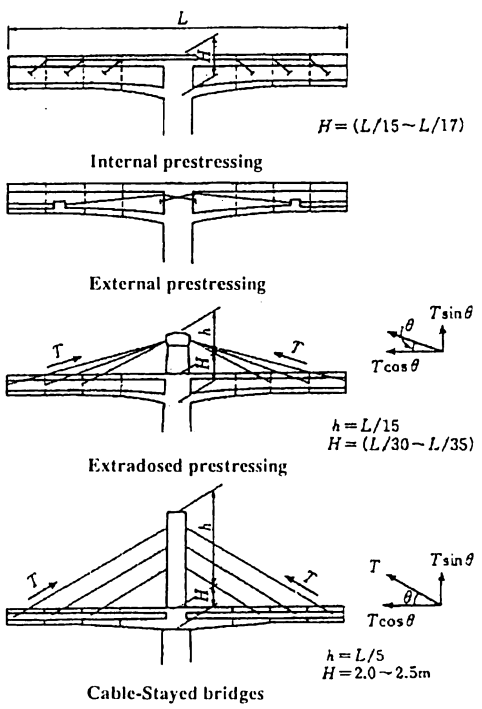


**Fig. 1-2 The evolution from box-girder bridge to cable-stayed bridges** [4]

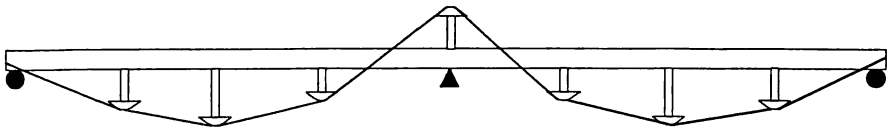

**External prestressing with large eccentricities**

**Fig. 1-3 Typical view of EPC beam with large eccentricities**

## 1.2 Literature Review

As mentioned earlier, in EPC structures there exists no bonding between concrete and prestressing tendons, hence, the compatibility condition of strain at critical section cannot be applied. This consequently makes the structural behavior dependent on the overall deformation of the structure, leading to much difficulty in the analytical method. Many previous researches have been extensively carried out to make clear understanding of the structural behavior of PC beam with external prestressing. In this section, only some of those investigations directly relevant to the present study are briefly reviewed comprising two main categories: flexural and shear behavior.

### 1.2.1 Flexural Behavior

Naaman (1989 [5]) proposed a simplified methodology for predicting the stress increase in unbonded tendons under service loading condition by using "*strain reduction coefficient*", $\Omega$, which is dependent upon only tendon profiles and types of loading. This methodology reduced the overall member analysis of PC beams with unbonded tendons to a sectional analysis at critical section. This concept was also extended to the ultimate flexural strength limit stage (Naaman, 1991 [6,7]) by the use of the ultimate strain reduction coefficient, $\Omega_u$, which was determined from a parametric study.

Vega and Doterppe (1988 [8]) analytically investigated the flexural behavior of internally unbonded PC beam by the use of moment-curvature method. They calculated the average tendon elongation by integrating the curvature, assuming the beam remains linearly elastic and uncracked throughout the stage of loading.

Virlogeux (1988 [9]) discussed many aspects about the flexural behavior of externally prestressed continuous and simply supported concrete beams. He proposed that the elongation of external tendon between two consecutive deviators can be calculated by considering the change of tendon's geometry under loading assuming the beam remains uncracked and linearly elastic. He also proposed a model for predicting the average tendon elongation at the ultimate stage using an expression for the length of plastic hinge.

Alkhairi and Naaman (1993 [10]) developed a nonlinear analytical model for the analysis of beams prestressed with unbonded tendons or external unbonded tendons. This model took into account the material nonlinearity, span-to-depth ratio, and second-order effect of eccentricity variation in external tendons. A good correlation between predicted and experimental results was indicated in this study.

Matupayont (1995 [11]) developed a similar analytical model for the analysis of PC beams with internal or external tendons both in simply supported and two-span continuous beams. This analytical model was also modified for precast segmental beams by simply modeling the joint behavior both in epoxy and dry joints. He also indicated that the secondary effect due to change of tendon's eccentricity can be reduced providing the arrangement of deviators at mid-span section is utilized, (Matupayont 1994 [12]).

Followings are some previous investigations related to the flexural behavior of precast segmental beams and secondary moment in continuous PC structures;

MacGregor et al. (1989 [13]) discussed about the flexural behavior of precast segmental structures by conducting an experimental program. The conclusion can be drawn that the overall behavior of segmental structures is completely dependent on the behavior of the joints, especially at critical joints where most of deformations are concentrated.

T.Y. Lin (1972 [14]) discussed the characteristic of secondary moment at the ultimate limit stage in continuous PC beams. He finally concluded that "if plastic moments with full redistribution are used to compute the ultimate load of a continuous beam, then secondary moments may be either neglected or included, since the results will be the same."

However, it should be noted that he mentioned only the ultimate flexural strength without consideration of bending moment profile along beam length which will be totally different in case of including or neglecting the secondary moment.

### 1.2.2 Shear Behavior

It has been known that experimental and analytical investigations of shear behavior of PC beams with external or internal unbonded tendons have been so far very few compared with that of flexural behavior. Some of previous researches can be reviewed as follows.

K. Kordina et al. (1989 [15]) experimentally investigated the shear strength of PC beams with internal unbonded tendons in order to study the effect of the bond condition. By comparing test results with shear design equations based on *truss model* and *tie-arch model*, they concluded that, in PC beam without bond, shear strength can be predicted accurately based on the concept of truss analogy which can distinguishes between tension-shear or flexural-shear failure and web-crushing failure.

Ito T. et al (1995 [16]) conducted an experimental program to investigate the shear strength of precast segmental T-shaped beams with external cables. Test results indicated that there was no diagonal cracks occurred in EPC beams, although the web thickness was thinner by 40% than that of similar PC beam with internal bonded tendons. This clearly demonstrated that external prestressing is very useful for increasing shear strength.

Tan K.H. and Ng, C.K. (1998 [17]) proposed an analytical model based on strut-and-tie model for calculating shear strength in EPC beam. Such a model was verified by test results and found to be accurately predictable for determining the ultimate load as well as the failure mode. From test results, they indicated that decreasing the concrete strength or the amount of shear reinforcement leads to shear-type failure and a correspondingly lower external tendon stress at ultimate strength of the beams. However, when an appropriate concrete strength and amount of shear reinforcement are provided, the beam would fail in flexure, even for shear span to effective depth ratio as lower as 2.5.

## 1.3 Objectives and Scope of Study

The concept of external prestressing with large eccentricities is quite new in the modern bridge constructions. To the best of author's knowledge, a clear understanding of the flexural behavior of this innovative type of structure has not yet been clarified regarding the ultimate flexural strength and force increase in external tendons especially in precast segmental beams. In order to obtain a better understanding of the flexural behavior of such beams, an experimental and analytical investigation was carried out in both single span and two-span continuous beams, emphasizing on the influence of casting method and the provision of internal unbonded tendon with external tendon. In addition an effect of shear loading type on this kind of structure was also investigated by conducting an experimental program of simply supported beams. The objectives of this study can be summarized as follows:

(a) to experimentally and analytically investigate the flexural behavior of EPC beams with large eccentricities both in monolithic and precast segmental beams,

(b) to make clear the applicability of deformation compatibility to the EPC beams with large eccentricities by comparing with a different concept based on the geometrical compatibility of external tendons,

(c) to experimentally investigate shear behavior of simply supported externally PC beams with large eccentricities both in monolithic and precast segmental beams.

# CHAPTER 2

# Experimental Methodology of Flexural Behavior of EPC Beams with Large Eccentricities

---

## 2.1 Introduction

The application of external prestressing with the precast segmental construction has been first developed since the construction of the Long Key Bridge in Florida, USA. Because of substantial cost and time saving in construction, this method has been extensively developed and efficiently used in many bridge structures. As mentioned in the previous chapter, the concept of external prestressing with tendon having large eccentricity has been recently investigated showing a considerable enhancement of the ultimate flexural strength comparing with that of conventional EPC beam. It is believed that this concept can also be applied to the precast segmental construction which is quite important for extending this application to the construction of highway bridge.

In order to obtain a better understanding of the flexural behavior of precast segmental beam externally prestressed with large eccentricities, an experimental program was carried out in both single span and two-span continuous beams. In addition, the effect of internal unbonded tendon was also investigated in single span beam with an emphasis on the ultimate flexural strength and the ductility of structure. This kind of combined prestressing method may be preferred in the precast segmental construction because there will be no problem concerning the quality of grouting concrete which has to be carried out in the case of using internal bonded tendon.

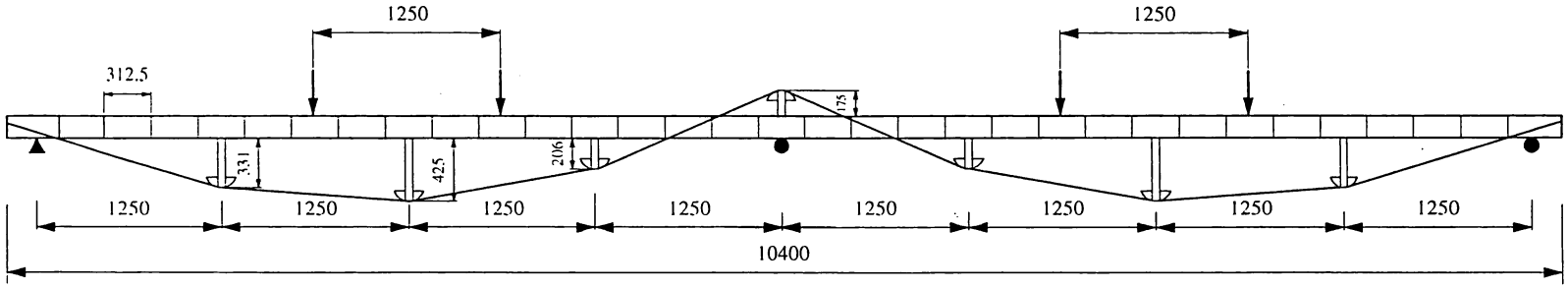


**Type A-1a**

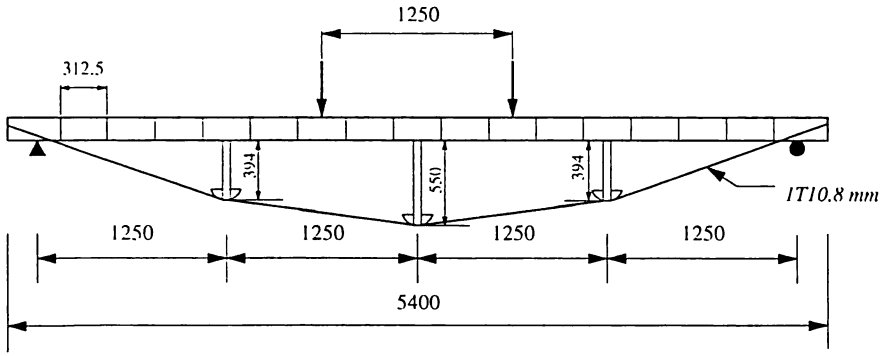


**Type D-1a**

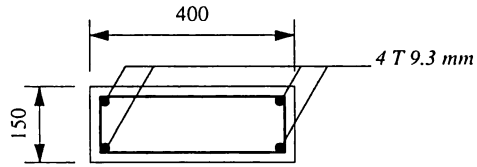


**Monolithic**

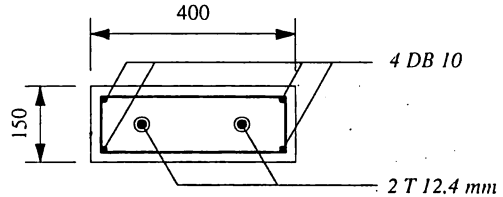


**Precast segment**

*(All dimensions in mm)*

**Fig. 2-1 Details of test beams (Precast Segmental)**

## 2.2 Details of Specimens and Test Variables

Test specimens consist of two main categories of single span beams with 5.00 m span length and two-span continuous beams with equal span length of 5.00 m. Each of them consists of monolithic and precast segmental beams with identical parameters for a comparison regarding the method of construction. All test beams were of rectangular-shaped concrete slabs having a depth and width of 150 mm and 400 mm respectively. The details of test variables and materials used in test are given in Table 2-1. The layout of test specimens and external tendons are shown in Fig. 2-1.

**Table 2-1 Summary of test variables and materials for flexure-type specimens**

| No. | Method of Casting | Type of Beam | Span Length (m) | Main Reinforcement | Prestressing Tendons | | Concrete strength, $f_c'$ (MPa) |
|---|---|---|---|---|---|---|---|
| | | | | | Internal (200 kN) | External (25 kN) | |
| A-1 | Monolithic | Two-span continuous | 2 x 5.00 | - | 4-T9.3 (Bond) | 1T10.8 | 51.9 |
| D-1 | | Single span | 2 x 5.00 | - | 4-T9.3 (Bond) | 1T10.8 | 57.2 |
| A-1a | Precast Segment, Epoxy joint | Two-span continuous | 5.00 | 4@DB10 | 2-T12.4 (Bond) | 1T10.8 | 67.1 |
| D-1a | | Single span | 5.00 | 4@DB10 | 2-T12.4 (Unbond) | 1T10.8 | 69.8 |

In single span beams, the layout of external tendon was provided in nearly parabolic shape, a general case of moment from external load, by means of deviating along three strut deviators which were connected to the concrete section at a spacing of 1.25 m. It is important to note that the provision of deviator at the mid-span can reduce the secondary effect in EPC structure regarding the change of tendon's eccentricity (Songkiat 1995 [13]). The ratio of span length to tendon depth is of 8 which is very low compared to those of conventional EPC beams. In precast segmental specimens, precast segments having 312.5 mm length were assembled with the provision of epoxy at the joints. The surface of each precast segments was provided with the multiple shear keys as shown in Fig. 2-2. Previous study (Guide, 1978[18]; Mathivat, 1983[19]) showed that the use of multiple shear keys can provide a better mechanical interlock, thus ensuring a more uniform transfer of stresses between the segments.

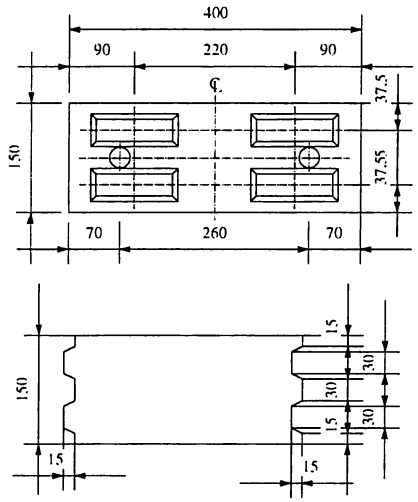


**Fig. 2-2 Details of shear keys in precast segmental beams**

## 2.3 Materials used for Test Specimens

### 2.3.1 Concrete

All the precast segments were cast in the PC factory and transported to the laboratory for testing. The method of casting is the long line match casting in which the first casting was done on the segments with even number by using the steel shear key plate as end formwork. One day later, the segments were removed from the formwork and the steam curing was carried out in order to gain the required strength. Since the first casting of segments had to be finished in one day due to the limited numbers of shear key-plate formwork, it was necessary to use a high early developed strength concrete. Subsequently, the segments with odd number were cast by using those of previous cast segments as formwork in order to provide a good interlock between each segment joints. The design strength of concrete, $f'_c$, was specified as 50 MPa in 28 days. The actual strength in each batch of casting was measured by the compressive test of sample with a diameter of 100 mm and height of 200 mm prepared during the step of concreting.

In specimens with internal bonded prestressing tendon, the grouting concrete was prepared by a concrete mix with a ratio of water to cement of 40 % and the air entrainment agent with a ratio of 2% by weight of cement was added in order to improve a workability. The

7-day compressive strength of the grouting concrete was measured by test of standard cylinder with 50 mm diameter and found to be around 20-30 MPa which is higher than the specified value of 17.3 MPa according to ACI 318-95 [20].

### 2.3.2 Reinforcements

The non-prestressed reinforcements with grade SD 345 of deformed bar with 10 mm diameter were used as the main longitudinal reinforcements and stirrup reinforcements. The mechanical properties of these reinforcements are given in Table 2-2. In monolithic beams, there was no main longitudinal non-prestressed reinforcements and the rectangular stirrups were provided at a spacing 100 mm along beam length except at the anchorages area where the spacing was reduced to 50 mm in order to prevent bond failure. In precast segmental beams, each segment was provided with main reinforcements at top and bottom layers and the stirrups were tied at spacing of 90 mm except at the anchorage segments in which the spacing of 50 mm was used. At the deviators location in all test specimens, the mesh reinforcement with a diameter of 3 mm was provided in order to prevent local compression failure due to force transfer from the strut deviators.

**Table 2-2 Mechanical properties of reinforcements**

| Type | Diameter (mm) | Sectional Area ($mm^2$) | Yielding Strength (MPa) | Young's Modulus (MPa) |
|---|---|---|---|---|
| SD 345 | 10 | 78.50 | 400 | 206,000 |

### 2.3.3 Prestressing Tendons

The prestressing tendons used for test specimens consist of two types of SWPR7A and SWPR7B with seven strands. The external tendons in all test beams were specified as the SWPR7B type with a diameter of 10.8 mm, but for internal tendons two different sizes were utilized. In monolithic beams, as the internal tendons were pre-tensioned at the time of casting, 4 tendons with a diameter of 9.3 mm were used. For precast segmental beams, in order to provide ease in assembly of segments, internal tendons were post-tensioned and the number was reduced to only 2 tendons with a diameter of 12.4 mm. It is noted that this

results in a reduction of total are of internal tendon in precast segmental beams about 10 % compared with those of monolithic beams.

**Table 2-3 Mechanical properties of prestressing tendons**

| Type | Sectional Area ($mm^2$) | Yielding Load (kN) | Ultimate Load (kN) | Young's Modulus (MPa) |
|---|---|---|---|---|
| SWPR7A - $\phi$ 9.3 mm | 51.61 | 75.5 | 88.8 | 194,000 |
| SWPR7B - $\phi$ 10.8 mm | 69.68 | 122 | 130 | |
| SWPR7B - $\phi$ 12.4 mm | 92.90 | 161 | 172 | |
| SWPR19N - $\phi$ 21.8 mm | 312.90 | 537 | 590 | 193,300 |

### 2.3.4 Epoxy Resin

Since the experiment was carried out during winter season, the winter-type epoxy resin using in precast segmental construction, PBAW type, was used for assembling precast segments. Before applying epoxy, the surface of segment joints was cleaned to remove the greasing material remained from the casting procedure by using wire brush and sand paper for obtaining a perfect bond condition at segment joints. After applying epoxy, the initial prestressing force around 50 kN was applied to provide initial confining force at the time of assembling the precast segments.

## 2.4 Instrumentation

During the conduction of the experimental program, various measuring devices were utilized in order to obtain necessary data such as concrete and steel strain, displacements of beam, force in prestressing tendon and applied load, etc. Each of these devices was selected by considering its appropriate function to measure the responses of beam under loading particularly at the critical sections. All measuring devices were connected to the switch boxes and a data logger in which a preliminary computation can be immediately carried out and the response of structure can be observed at the time of loading. The details of these instrumentation are provided in following section.

### 2.4.1 Strain Gages

Two types of electrical resistance strain gages were used for measuring the strain in concrete and steel reinforcements. Gages with 2 mm length were used for measuring strain in both ordinary reinforcements and prestressing tendons because they were suitable for the measurement of a very small change in length at a particular point along the length of reinforcing steel. Whereas in the measurement of concrete strain, because it is not possible to specify the location where the largest change of strain would occur, gages with 60 mm were attached at the concrete surface of the expected critical sections.

### 2.4.2 Displacement Transducers

The cambers during initial prestressing as well as the vertical deflections of beams under loading were measured by the use of displacement transducers. These devices varying in length from 50 to 200 mm were mounted at the important locations along the beam length, which were the center of loading span, the deviators location and the loading points in each span, in order to monitor the vertical deflections as well as the change of tendon's eccentricity. Moreover, a horizontal displacement typically called "$\pi$" gage was also utilized for measuring a crack width or joint openings in precast segmental beams. Two different sizes consisting of 100 and 150 mm length were selected depending on the expected size of crack or joint opening.

### 2.4.3 Load Cells

Load cells were used for measuring the applied force by placing between the loading jack and the load-transferring girder. Furthermore, they were also mounted at the anchorage ends of prestressing tendons in order to monitor the force increase in prestressing tendons. The support reactions in two spans continuous beams were also measured by placing two load cells per support below the beam in order to monitor the occurrence of moment redistribution which is a very important characteristic in statically indeterminate structures.

## 2.5 Prestressing Method

All test specimens were prestressed with a mixed prestressing system consisting of external and internal prestressing. The amount of initial prestressing force for external and internal tendons was approximately 25 kN (18% $f_{pu}$) and 200 kN (55% $f_{pu}$) respectively. The provision of internal tendon was mainly designed for preventing cracking in concrete at outmost fiber during the transportation as well as when introducing external prestressing force. In monolithic beams, the internal tendons were straightly arranged into two levels with the depths of 4 and 11 cm from the top fiber of concrete section and were pre-tensioned at the factory. Nevertheless, the internal tendons in precast segmental beams were placed at the mid-depth level of concrete section and were post-tensioned during assembling the precast segments. For two spans continuous beam (A-1a type), the grouting was later carried out in order to provide a bond between internal tendons and surrounding concrete sections, making a similar condition as in beam A-1. However, in single span beam (D-1a), the grouting of internal tendon was not carried out in order to make a comparison on the effect of internal unbonded tendon with beam D-1 provided with pre-tensioned internal bonded tendons.

# CHAPTER 3

# Experimental Results of Flexural Behavior of EPC Beams with Large Eccentricities

## 3.1 Introduction

An experimental program of flexural behavior of EPC beams with large eccentricities was conducted with the details as described in the previous chapter. The main objective is to investigate the applicability of using external tendons with large eccentricities to the precast segmental beams which are considered as a greatly advantageous construction method of bridge structures. Furthermore the effect of internal unbonded tendons was also investigated by comparing with the identical beam provided with internal bonded tendons. These experimental results are presented and discussed in this chapter with emphasis on the ultimate flexural strength, the ultimate deformation or ductility and the force in external tendons. Besides, in two-span continuous beam, the moment redistribution mechanism was also discussed as it has a marked influence on the overall flexural behavior of statistically indeterminate structures.

## 3.2 Ultimate Flexural Strength

The experimental results including cracking loads, ultimate loads and mode of failure of single span beams and two-span continuous beams are summarized in Table 3-1 and 3-2 respectively. It should be noted that cracking loads in precast segmental beams were defined as the applied loads that caused joint opening at critical sections. It can be seen that, in single span beams, the cracking loads of monolithic (37.0 kN) and precast segmental beams (36.3 kN) are nearly the same, indicating the same flexural behavior up to the occurrence of cracking. This similarity was also obtained in the test series of two-

span continuous beams (A-type). This similar elastic behavior is mainly due to the application of epoxy resin at segment joints in precast segmental beams resulting in higher tensile strength at the joint, hence, cracks can occur in concrete adjacent to the segment joints. In two-span continuous beams, cracking was firstly observed at the center support region and subsequently at the mid-span regions in both spans. This is because the applied moment from external load at the center support was higher than that of mid-span regions in case of two-span continuous beam. It should be noted that, in beam A-1a, cracking load at right span (44.7 kN) was slightly higher than that of left span (38.7 kN). This can be attributed to the different concrete strengths of critical segmental blocks in each span which are 60.9 MPa and 59.8 MPa for right and left span respectively.

**Table 3-1 Summary of test results of single span beams (D-type)**

| No. | Description | Cracking Load (kN) | Ultimate Load (kN) | Mode of Failure |
|---|---|---|---|---|
| D-1 | Single span Monolithic | 37.0 | 94.5 | Crushing of concrete at right loading point, Ext. tendon: yielded, Int. tendon: yielded |
| D-1a | Single span Precast segment | 36.3 | 86.3 | Crushing of concrete at right loading point, Ext. tendon: yielded, Int. tendon: not yielded |

**Table 3-2 Summary of test results of two-span continuos beams (A-type)**

| No. | Description | Cracking Load (kN) | | | Ultimate Load (kN) | | Mode of Failure |
|---|---|---|---|---|---|---|---|
| | | Left span | Center support | Right Span | Left span | Right Span | |
| A-1 | Two-span Monolithic | 39.2 | 36.8 | 39.2 | 107.9 | 108.6 | Crushing of concrete, Yielding of external tendon |
| A-1a | Two-span Precast segment | 38.7 | 37.7 | 44.9 | 99.2 | 101.0 | Crushing of concrete, Yielding of external tendon |

The failure mode of all test beams can be defined as the flexural compression type due to the crushing of concrete at critical sections. In single span beams, crushing of concrete was observed at the right loading point, and the ultimate flexural strength of monolithic beam (D-1) was higher than that of segmental beam (D-1a) approximately 8%. This can be attributed to the effect of internal unbonded tendon in beam D-1a, resulting in lower ultimate internal tendon force compared to that of beam D-1. In other words, it can be clearly seen that there was no yielding of internal tendon in beam D-1a at the ultimate stage. It is also noted that the ultimate flexural strengths given in Table 3-1 and 3-2 were

defined as the applied load when the crushing of concrete at critical sections was observed in the tests.

In two-span continuous beams, crushing of concrete was observed at the top fiber of concrete section (A-1) or segment joints (A-1a) under the loading point in the left span and internal tendons were yielded. Note that there was no crushing of concrete at the bottom fiber of concrete section or joints at the center support. It is resulted from higher magnitude of resisting moment from external prestressing at the center support due to the effect of secondary moment. The ultimate loads of beam A-1 and A-1a were slightly different having the average value of 108.3 kN and 100.1 kN respectively. This difference is due to the lower total area of internal bonded tendons in segmental beam (A-1a), approximately 10% less than that of monolithic beam (A-1).

The load-deflection relationships of single span and two-span continuous beams were shown in Fig. 3-1 and 3-2 respectively. It can be seen that in all test beams the load-deflection curves can be divided into three major portions as: 1) linear elastic uncracked, 2) linear elastic cracked and 3) nonlinear cracked. In the first portion, the response of beam under loading behaves linearly up to the first occurrence of cracking or joint opening in segmental beams. This elastic linear behavior is almost the same by comparing between monolithic and precast segmental beams in each series of single span and two-span continuous beams. After the occurrence of cracking, the slope of load-deflection curve is rather higher than that in previous stage because of the reduction of flexural stiffness of cracked concrete section. However the responsive curves still showed a linear relationship in this stage. This is because the external tendons, which give a large contribution to the flexural strength of this kind of structure, remain in the elastic range as can be observed from the force measured by load cells in the tests.

It is also essential to note that the load-deflection curve of monolithic beams registered slightly higher slope compared to that of precast segmental beams. This behavior can be mainly attributed to the discontinuity characteristics of precast segmental beams due to the existence of segment joints along beam length. After the occurrence of joint opening, it was observed that, cracks continuously propagated only at the critical joints (see Fig. 3-3),

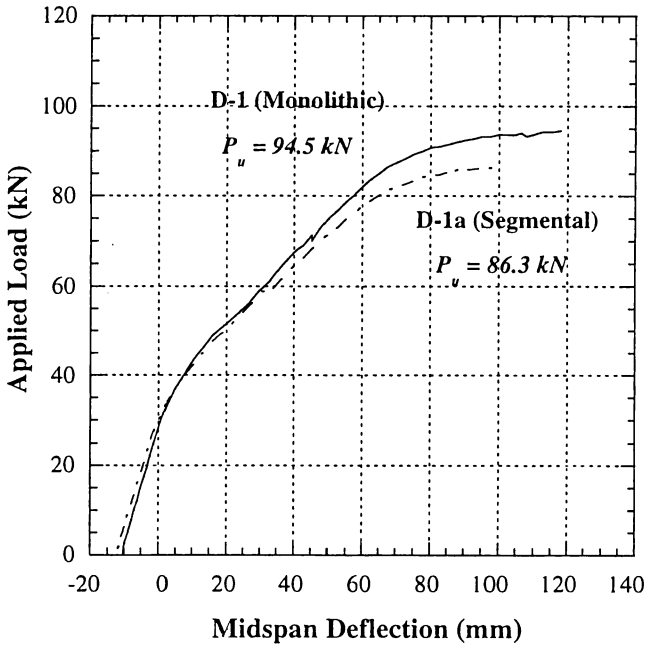


**Fig. 3-1 Load-deflection relationship of single span beams (D-type)**

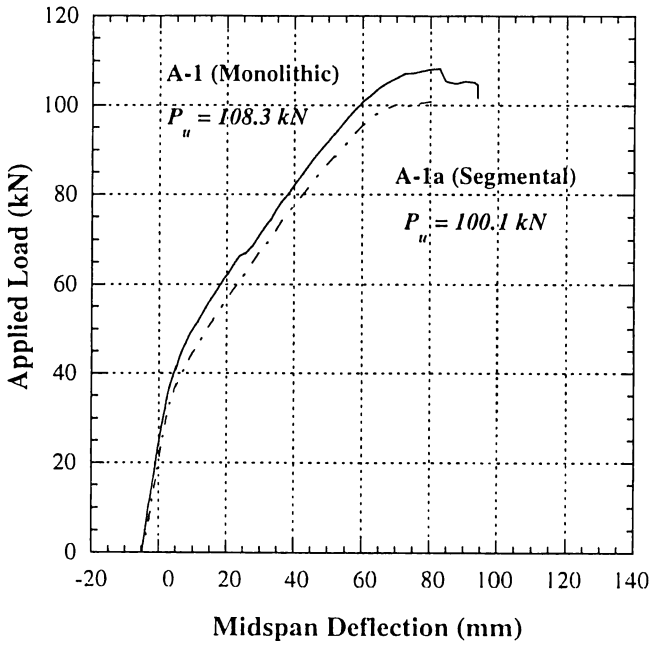


**Fig. 3-2 Load-deflection relationship of two-span continuous beams (A-type)**

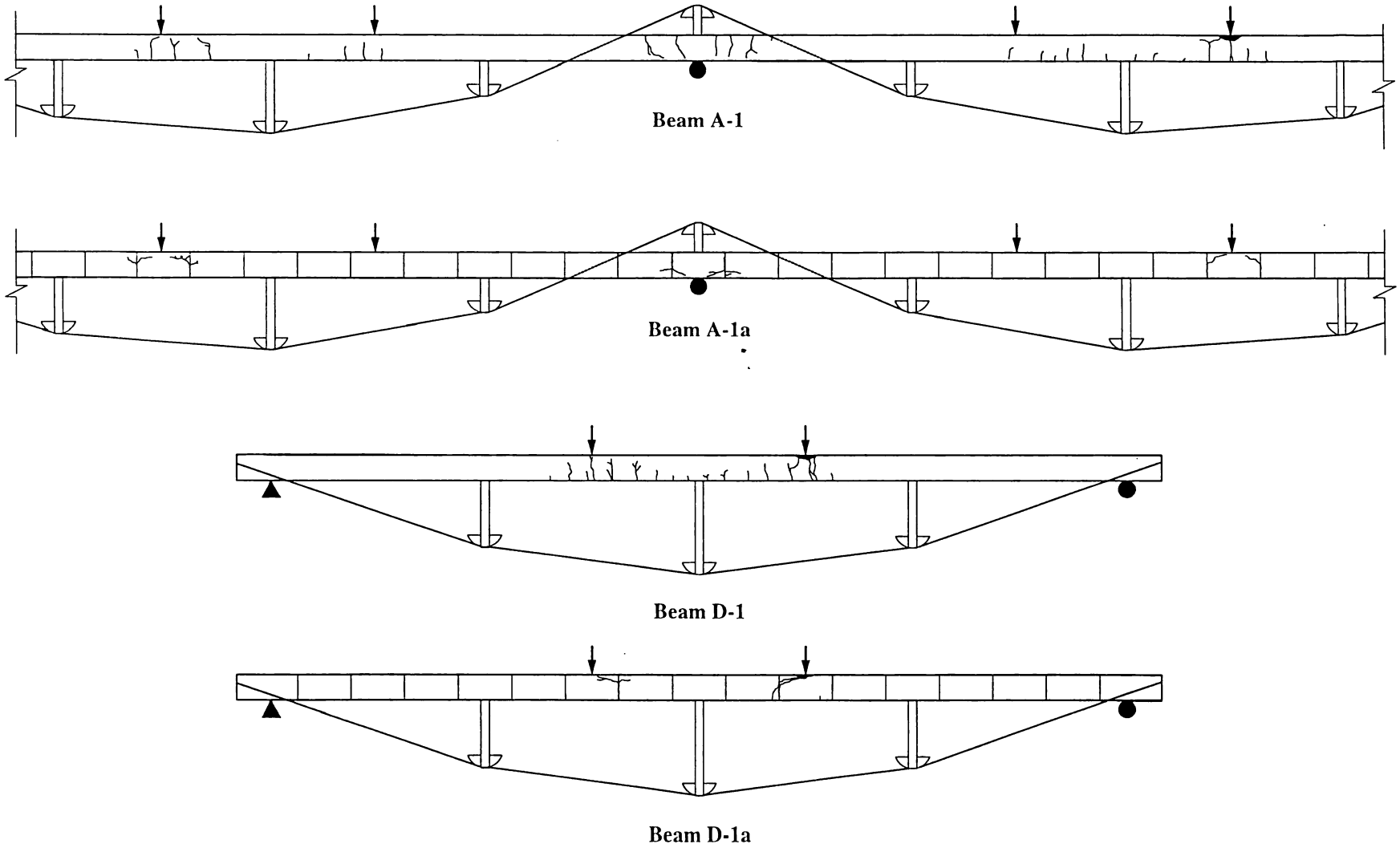


**Fig. 3-3 Crack pattern of flexure-type specimens**

as load was increased, causing a concentration of rotation and compressive concrete strain and eventually resulting in larger deflection than that of monolithic beams in which cracks can further occurred at other stiffer sections. Considering the nonlinear cracked behavior near the ultimate stage, it is clearly observed that the load-deflection responses of all test beams show very large increment of deflection with a little increase of applied load, indicating a ductile behavior of structure. This is because force in external tendons can be increased up to the yielding as a consequence of the provision of large eccentric external tendons in this type of structure.

## 3.3 Ultimate Deflection and Ductility

The summary of deflections of all test beams at important stages of loading is given in Table 3-3.

**Table 3-3 Summary of deflections observed in test**

| No. | Description | Initial camber (mm) | | Deflection at crushing of concrete (mm) | | Maximum deflection (mm) | |
|---|---|---|---|---|---|---|---|
| | | Left span | Right span | Left span | Right span | Left span | Right span |
| A-1 | Two-span, Monolithic | -4.9 | -4.9 | 82.7 | 82.6 | 94.1 | 93.8 |
| A-1a | Two-span, Segmental | -3.6 | -3.8 | 70.2 | 70.1 | 80.1 | 80.0 |
| D-1 | Single span, Monolithic | -10.7 | | 117.9 | | 130.3 | |
| D-1a | Single span, Segmental | -12.3 | | 100.2 | | 100.2 | |

It can be seen that the initial camber of single span beams was around 11 mm while it was only about 4.5 mm in two-span continuous beams. This is due to the fixed condition at the center support in two-span continuous beams whereas the rotational capacity can be obtained in single span beams. It can be seen that the deflections at crushing of concrete in monolithic beams were larger than that of precast segmental beams. Similarly, the maximum deflection in monolithic beams was slightly higher than the value at crushing of concrete compared to the precast segmental beams. The reason for these characteristics is that in precast segmental beams there was a concentration of compressive concrete strain at the critical joints leading to an earlier failure mechanism. Whereas in monolithic beams, after the concrete crushing at the top compressive fiber of critical sections, beams can still additionally resist some magnitude of load by the uncrushed adjacent concrete section resulting in non-sudden failure mode unlike in precast segmental beams.

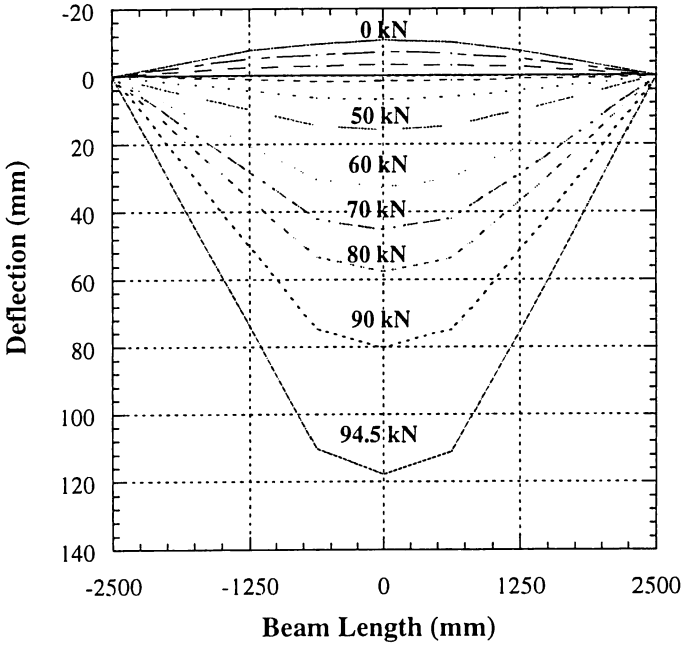


(a) Beam D-1 (monolithic)

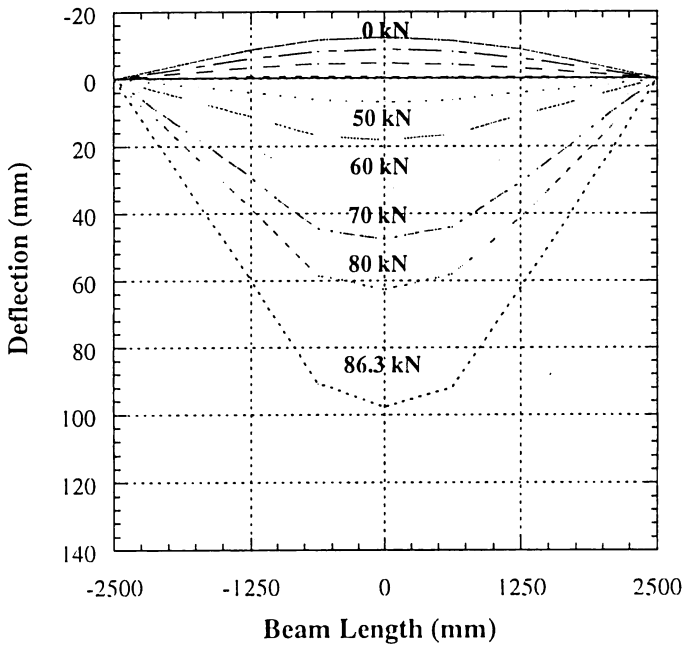


(b) Beam D-1a (precast segment)

Fig. 3-4 Deflection along beam length of single span beams (D-type)

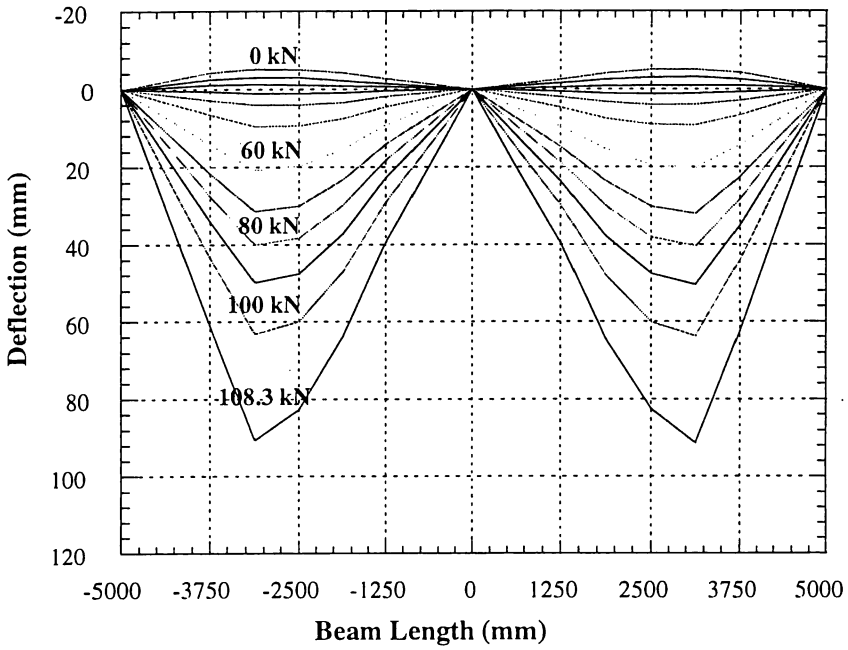


(a) Beam A-1 (two-span and monolithic)

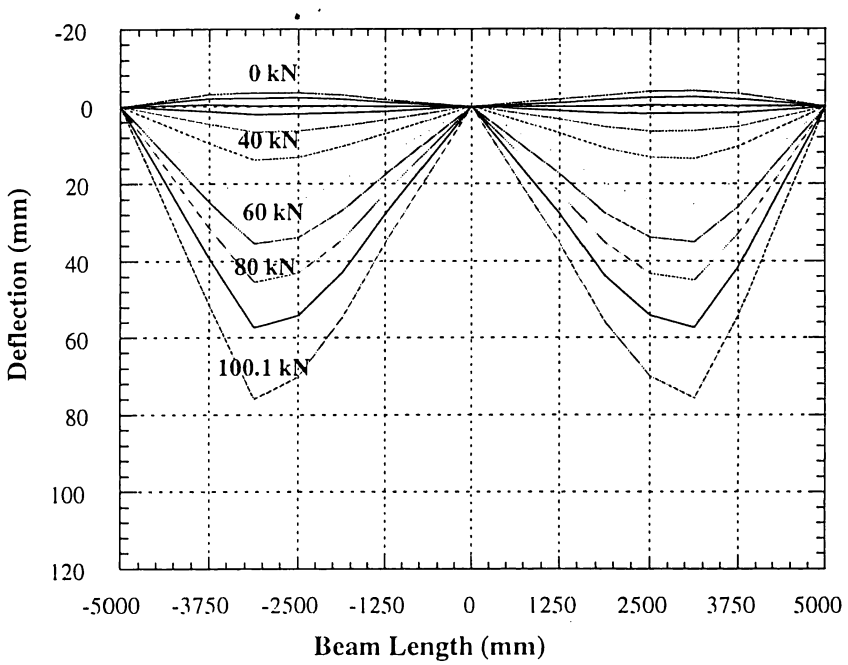


(b) BeamA-1a (two-span and precast segment)

Fig. 3-5 Deflection along beam length of two-span continuous beams (A-type)

The profiles of deflection along beam length are shown in Fig. 3-4 and 3-5 for single span beams and two-span continuous beams respectively. It can be seen that the maximum deflection was at mid-span region in single span beams while it was at the outside loading point in each span of two-span continuous beams. This can be attributed to the shape of the applied moment from external load which is largest at the loading point in two-span continuous beams. It can also be seen that the deflections on both spans in two-span continuous beams had almost the same value implying that the loading system was effectively symmetrically applied in the experimental program.

## 3.4 Force in Prestressing Tendons

The variation of force in unbonded tendon is a very important parameter in PC structure as it depends on the overall behavior of structure not only at critical section. In order to measure the change of force in both external tendons and internal unbonded tendons, load cells were attached at the end anchorages. Further, the electronic strain gages were also attached at the critical locations to monitor the strain increase of internal bonded tendons. The summary of initial prestressing force and the ultimate tendon force of both external and internal tendons is shown in Table 3-4.

**Table 3-4 Summary of force in prestressing tendons at important stages**

| No. | Description | External tendon | | | | | Internal tendon | | |
|---|---|---|---|---|---|---|---|---|---|
| | | Initial PS force (kN) | | Ultimate tendon force (kN) | | Yielding | Initial PS force (kN) | Ultimate tendon force (kN) | Yielding |
| | | Left end | Right end | Left end | Right end | | | | |
| A-1 | Two-span, monolithic | 26.2 | 25.4 | 116.0 | 115.8 | Yielded | 205.3 | > 303.8 | Yielded |
| A-1a | Two-span, segmental | 23.9 | 24.8 | 109.9 | 107.9 | | 200.4 | > 294.6 | |
| D-1 | Single span, monolithic | 24.7 | 24.7 | 117.9 | 118.3 | | 192.9 | > 303.8 | |
| D-1a | Single span, segmental | 23.8 | 23.5 | 114.4 | 114.1 | | 196.2 | 222.8 | Not yielded |

As can be seen from Table 3-4, the external tendons were yielded in all specimens indicating an effective utilization of prestressing tendons in this kind of structure. The measured ultimate external tendon force at both end anchorages showed nearly the same value with the maximum difference of 2%. This means that the effect of friction force at

deviators was of insignificance and can be neglected in the analytical method. It is important to point that, except beam D-1a, the internal tendons also reached yielding at the ultimate stage. In beam D-1a, as the grouting of internal tendon was not carried out resulting in an unbonded condition, therefore, the tendon force can be increased only by 26.6 kN or approximately 9% $f_{py}$.

The response of force in external tendons at any stage of loading of all specimens is shown in Fig. 3-6. It can be clearly seen that the rate of force increase in external tendon with applied load is comparatively higher in single span beams than that of two-span continuous beams. This can be attributed to the larger deflection at any step of loading in single span beams, consequently resulting in the greater elongation of external tendons. Considering between monolithic and precast segmental beams, it was found that force in external tendons in the latter one register slightly higher rate of increase than the former. This characteristic was also due to the difference of deflection shape which is slightly larger in precast segmental beams as described in previous section.

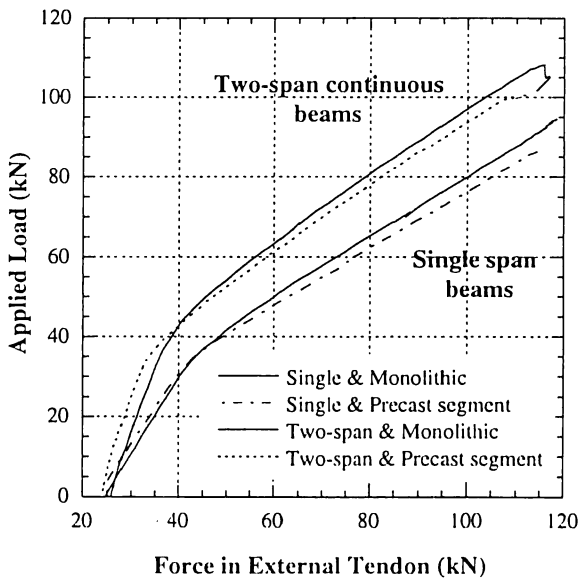


**Fig. 3-6 Applied load and force in external tendons relationship**

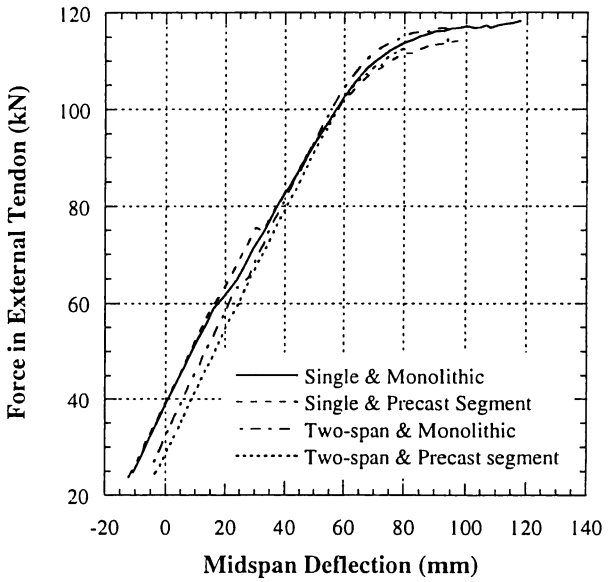


**Fig. 3-7 Force in external tendons and mid-span deflection relationship**

It is very interesting to note that, from Fig. 3-7, there is the same relationship between force in external tendons and mid-span deflection in both single span and two-span continuous beams. Before reaching the yielding point, the relationship is almost linear implying that the external tendons were in elastic range. Afterwards the curve showed a very steep slope indicating the start of yielding of external tendon. This similar behavior can be explained by considering that the geometrical shape or layout of external tendons in both single span and two-span continuous beams was designed to be identical, so the change of shape of external tendons due to a unit of mid-span deflection will be the same, consequently resulting in the same magnitude of force increase in external tendons as observed in Fig. 3-7.

## 3.5 Moment Redistribution in Two-span Continuous Beams

It is generally known that the influence of moment redistribution in statically indeterminate structure having sufficient ductility at critical sections is very important as it greatly affects the ultimate flexural strength of the structure. To investigate this phenomena, the support reactions were measured in the tests by means of placing load cells under concrete beam at each support. The relationship between support reactions and the applied load is illustrated

in Fig.3-8 (a) and (b) for monolithic beam (A-1) and precast segmental beam (A-1a) respectively. In addition, the calculated support reactions if the beams behave elastically are also given for making a clear comparison of moment redistribution behavior. It can be observed that the curves between support reactions and the applied load had a nearly bilinear shape where the deflected point was indicated at load approximately of 35 kN in both beam A-1 and A-1a. This magnitude of load can be regarded as the cracking load at center support observed in the tests, implying that the start of non-linear behavior or moment redistribution can be defined as when the occurrence of concrete cracking at center support. It can also be seen that at any stage of loading, the observed values of center support reactions were lower than the calculated elastic values, and the opposite case for the end support reactions. It can be concluded that after the occurrence of cracking at center support, the additional applied moment was transferred to the mid-span sections.

**Table 3-5 Summary of ultimate moments and percentage of moment redistribution**

| No. | Observed plastic moment $M_p$ (kN-m) | | | Calculated elastic moment $M_e$ (kN-m) | | | Moment redistribution (%) $[1-M_p/M_e]$ | | |
|---|---|---|---|---|---|---|---|---|---|
| | Left Span | Center Support | Right span | Left Span | Center support | Right Span | Left span | Center support | Right span |
| A-1 (monolithic) | 75.8 | -67.8 | 76.3 | 65.8 | -95.1 | 65.8 | -15.2 | 28.7 | -16.0 |
| A-1a (precast segment) | 71.4 | -59.5 | 71.7 | 60.9 | -88 | 60.9 | -17.2 | 32.4 | -17.7 |

The magnitude of moment redistribution can be evaluated by comparing the plastic moment, $M_p$, calculated by observed support reactions with the elastic moment, $M_e$, computed by assuming elastic behavior. The summary of ultimate moments of beam A-1 and A-1a is given in Table 3-5. The bending moment profiles along beam length are also illustrated in Fig.3-9. It can be seen from Table 3-5 that the observed moments at the mid-span were higher than that of the elastic moments showing a negative redistribution. On the contrary, the positive redistribution was obtained at center support indicated by the lower observed plastic moment compared to the calculated elastic moment. Comparing between beam A-1 and A-1a, it was found that the percentage of redistribution at center support was slightly higher in precast segmental beam (32.4 %) compared to the monolithic one (28.7 %). This difference can be attributed to a large concentrated joint-rotation at the center support in segmental beams resulting a marked redistribution of moment.

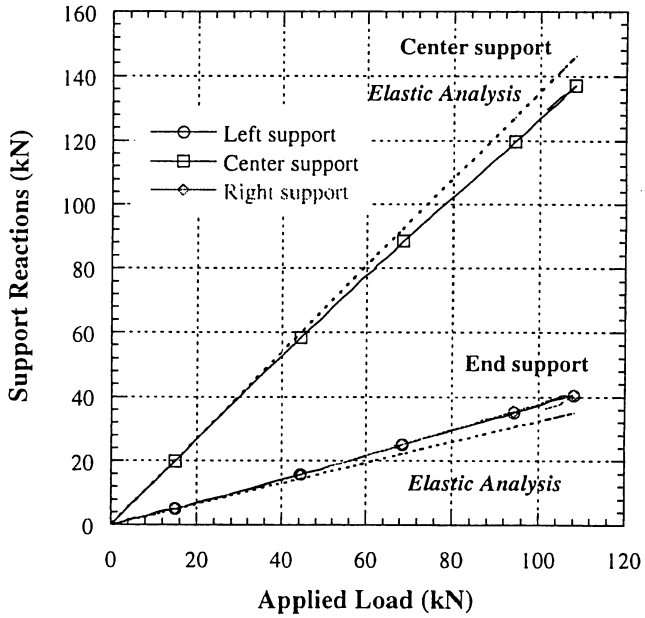


(a) Beam A-1 (monolithic beam)

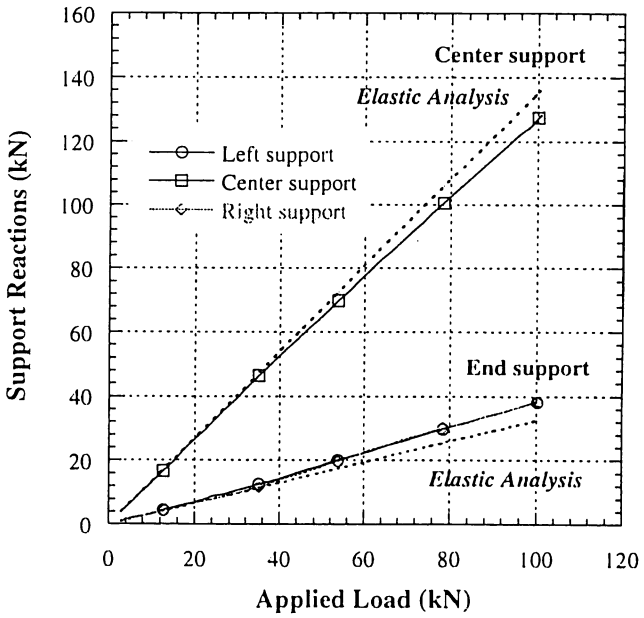


(b) Beam A-1a (precast segmental beam)

**Fig. 3-8 Relationship between support reactions and applied load**

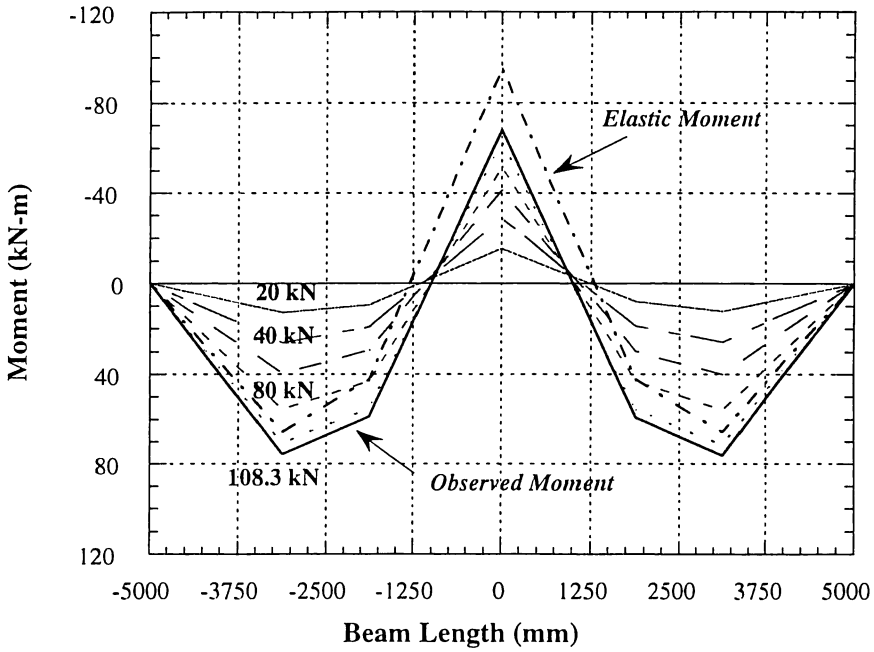


(a) Beam A-1 (monolithic beam)

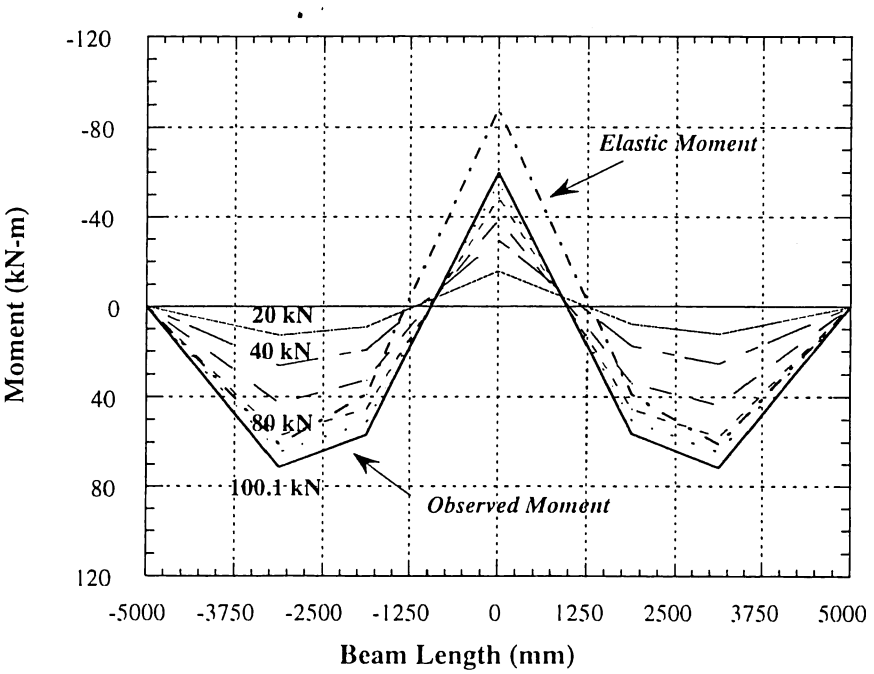


(b) Beam A-1a (Precast segmental beam)

**Fig. 3-9 Bending moment profile along beam length at various loading steps**

## 3.6 Conclusions

It can be concluded from the test results discussed in this chapter that the flexural behavior of externally PC beams with large eccentricities was basically nearly the same for both monolithic and precast segmental beams. By placing external tendon at large eccentricities force in external tendon can be increased up to the yielding point indicating an effective utilization of prestressing tendons in this type of structure. Nonetheless, some considerations should be also given to the serviceability condition in which the cracking load was observed to be rather lower compared to the ultimate load. The relationship between force in external tendon and mid-span deflection was found to be the same in both single and two-span continuous beams which had a linear relationship before the external tendons yielded. The effect of internal unbonded tendon was found to be small on the ultimate flexural strength and ultimate deflection. In addition the moment redistribution in two-span continuous beams was slightly larger in precast segmental beam than that of monolithic one due to the influence of concentration of compressive strain which caused larger rotation at critical joints. By considering these characteristics, an analytical methodology based on the moment-curvature method was proposed and, finally, a comparison between experimental versus analytical results was discussed in next chapter.

# CHAPTER 4

# Analytical Methodology of Flexural Behavior of EPC Beams with Large Eccentricities

---

## 4.1 Introduction

It has been generally known that the flexural analysis of EPC beams has an additional difficulty regarding force increase in external tendon which depends upon the overall structure, *member-dependent,* rather than the critical section as usually used in conventional flexural analysis. Previous researches carried out by Alkhairi and Naaman (1993 [10]) and Matupayont (1995 [11]) have shown that by using the concept of *deformation compatibility* along with the conventional beam theory, the flexural strength as well as the stress in external tendon could be predicted with a good accuracy. This methodology was also extended for the analysis of EPC beam with large eccentricities by Aravinthan, et al. (1999 [2]) by adopting an assumption considering imaginary concrete strain at tendon level, and was verified by comparing with the experimental results showing a good accuracy. However, such an applicability may have a limitation when the eccentricity of external tendon becomes very large. In order to make a clear understanding of such a concept, an analytical investigation was carried out in this study.

## 4.2 Basic Assumptions

A nonlinear analytical methodology used for analyzing the flexural behavior of EPC beams with large eccentricities was essentially adopted from the moment-curvature method with multiple iterative loops. The fundamental assumptions used in the analytical method can be summarized as follows:

(1) Plane section remains plane after bending (Bernoulli theory of bending). This implies that the variation of strain normal to the plane of the concrete section can be assumed to be linear through the depth.

(2) Strain in external or unbonded tendon is uniformly distributed along its entire length. In other words, the influence of friction force at the surface between tendons and deviators is neglected.

(3) The total elongation of external tendon is equal to the total deformation of concrete strain at tendon level (*the compatibility of deformation*).

(4) The provision of web reinforcement is sufficient to resist shear force and has no contribution to the flexural strength of beam.

(5) The shear deformation is neglected.

It should be noted that assumption (3) has been verified to be applicable for the analysis of conventional EPC structures by many previous researchers. For extending such a concept to the beam with large eccentric tendon in which a major portion of tendon is placed considerably far from the concrete section, an additional assumption was also adopted considering the imaginary concrete strain at the tendon level (Fig.4-1).

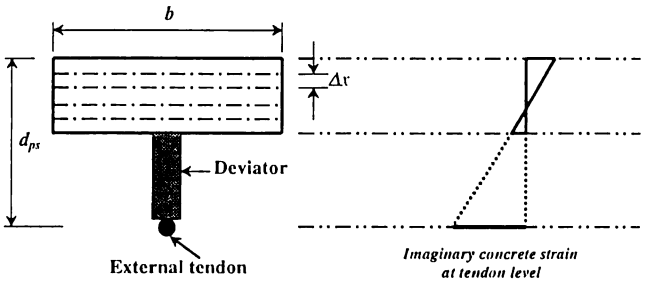


**Fig. 4-1 Imaginary concrete at tendon level**

## 4.3 Analytical Methodology of Single Span Beams

### 4.3.1 Overview

It has been commonly known that the analysis of EPC beam cannot be determined by performing an analysis of the critical section, *section-dependent*, but it should be evaluated from the overall behavior of the structure, *member-dependent*, (Naaman, 1993 [6]) which requires much more effort due to the complex iterative calculations. As such, a

comprehensive analytical method was carried out by using computer programming written in FORTRAN language initially developed by Matupayont (1995 [11]). Several factors such as the nonlinear behavior of materials an the geometry of unbonded tendon were taken into account in the analytical program. It is noted that the geometrical nonlinearity of unbonded tendon was considered due to the fact that the deflected shape of unbonded tendon will not follow the deformation of structure, leading to the change of tendon's eccentricity except at the deviations and anchorages.

### 4.3.2 Constitutive Models of Materials

The idealized stress-strain relationships of materials used in the analytical program were considered the nonlinearity behavior. This is because the overall flexural behavior of EPC beam up to the ultimate stage can be more accurately predicted than that based on the elastic relationship of material. The details of constitutive models of all materials are given as follows.

#### (a) Concrete

The modified Hognestad stress-strain curve was used as a constitutive model for concrete in compressive stress consisting of a parabolic curve followed by the sloping line and terminating at a limiting strain, $\varepsilon_{cu}$, as shown in Fig. 4-2. In the tensile stress, it should be noted that after the stress in concrete reaches the modulus of rupture,$F_r$, it is assumed that concrete can still resist more tensile stress until the ultimate tensile strain, $\varepsilon_{tu}$, which can be referred as the commencement of cracking.

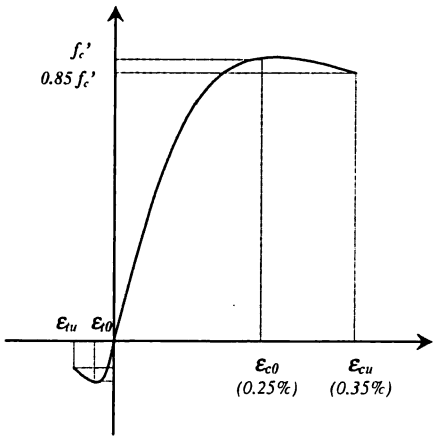


**Fig. 4-2 Stress-strain relationship of concrete**

The equations of constitutive models of concrete are given as follows:

$$\begin{aligned}
\sigma_c &= f_c'\left[2\varepsilon_c/\varepsilon_{c0} - (\varepsilon_c/\varepsilon_{c0})^2\right] && for\ 0 \le \varepsilon_c \le \varepsilon_{c0} \\
&= (\varepsilon_c - \varepsilon_{cu})(F_{cu} - f_c')/(\varepsilon_{cu} - \varepsilon_{c0}) + F_{cu} && for\ \varepsilon_{c0} < \varepsilon_c \le \varepsilon_{cu} \\
\sigma_c &= -F_r\left[2|\varepsilon_c|/\varepsilon_{t0} - (|\varepsilon_c|/\varepsilon_{t0})^2\right] && for\ 0 \le |\varepsilon_c| \le \varepsilon_{t0} \\
&= (|\varepsilon_c| - \varepsilon_{tu})(F_{ru} - F_r)/(\varepsilon_{tu} - \varepsilon_{t0}) + F_{ru} && for\ \varepsilon_{t0} \le |\varepsilon_c| \le \varepsilon_{tu} \\
F_{cu} &= 0.85f_c' \\
F_r &= 0.58(f_c')^{2/3} \\
F_{ru} &= 0.85F_r \\
E_c &= 40000(f_c')^{1/3}
\end{aligned} \qquad \textbf{(4-1)}$$

in which:

$f_c'$ = maximum compressive strength of concrete, kgf/cm$^2$

$F_{cu}$ = ultimate compressive strength of concrete (at crushing), kgf/cm$^2$

$F_r$ = modulus of rupture of concrete, kgf/cm$^2$

$F_{ru}$ = ultimate tensile strength of concrete (at cracking), kgf/cm$^2$

$E_c$ = modulus of elasticity of concrete, kgf/cm$^2$

**(b) Reinforcements**

The stress-strain relationship of reinforcements is assumed to be bilinear characteristic having perfectly plastic behavior after yielding as shown in Fig. 4-3.

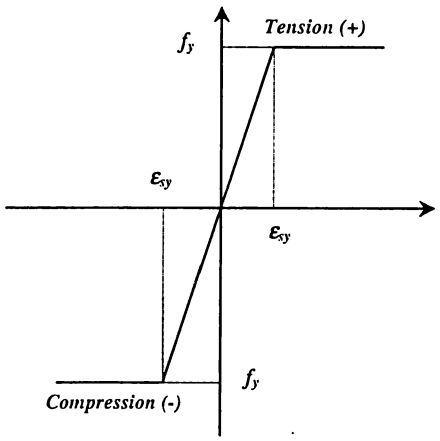


**Fig. 4-3 Stress-strain relationship of reinforcements**

in which

$E_s$ = modulus of elasticity of reinforcing steel

$f_y$ = yield strength of reinforcing steel

### (c) Prestressing Tendons

It should be noted that in EPC beam with large eccentricities, stress in external tendon can be substantially increased as load increasing and may reach up to the yield strength at the ultimate stage due to its large eccentricity. Therefore, a constitutive model that can accurately predict the overall nonlinear behavior of prestressing steel is important. In this study, the stress-strain relationship of prestressing steel was adopted from that proposed by Menegotto and Pinto, 1973 [22] which has a smooth change from elastic to plastic behavior as shown in Fig. 4-4.

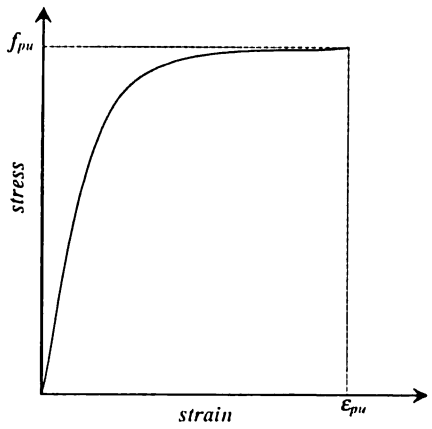


**Fig. 4-4 Stress-strain relationship of prestressing tendons**

The expression of equation can be given as following:

$$f = E_{ps}\varepsilon_{ps}\left[Q + \frac{1-Q}{\left\{1+\left(\frac{E_{ps}\varepsilon_{ps}}{Kf_{py}}\right)^{N}\right\}^{1/N}}\right] \text{ and } Q = \frac{f_{pu} - Kf_{py}}{E_{ps}\varepsilon_{pu} - Kf_{py}} \quad \textbf{(4-2)}$$

with the following parameters;

$N = 4.77$, $K = 1.1341$

$f_{py} = 0.85 f_{pu}$

$E_{ps} = 1.90 \times 10^6$ kgf/cm$^2$ (27,000 ksi)

$\varepsilon_{pu} = 0.040$

where:

$E_{ps}$ = modulus of elasticity of prestressing tendon

$f_{py}$ = yield strength of prestressing tendon

$f_{pu}$ = ultimate strength of prestressing tendon

$\varepsilon_{pu}$ = ultimate strain of prestressing tendon

### 4.3.3 Flowchart of Analytical Program

The flowchart of the analytical program is given in Fig.4-5. It can be seen that the step of calculation can be mainly categorized into three major iterative loops as 1) force equilibrium condition, 2) moment equilibrium condition, and 3) compatibility of unbonded tendon. The analytical model of simply supported beam used in this program is shown in Fig. 4-6. The beam is divided longitudinally into subdivision of $n$ elements. The integration points, $i$, are defined as the locations between each elements which can be also interpreted as the locations of uniformly distributed crack along beam length.

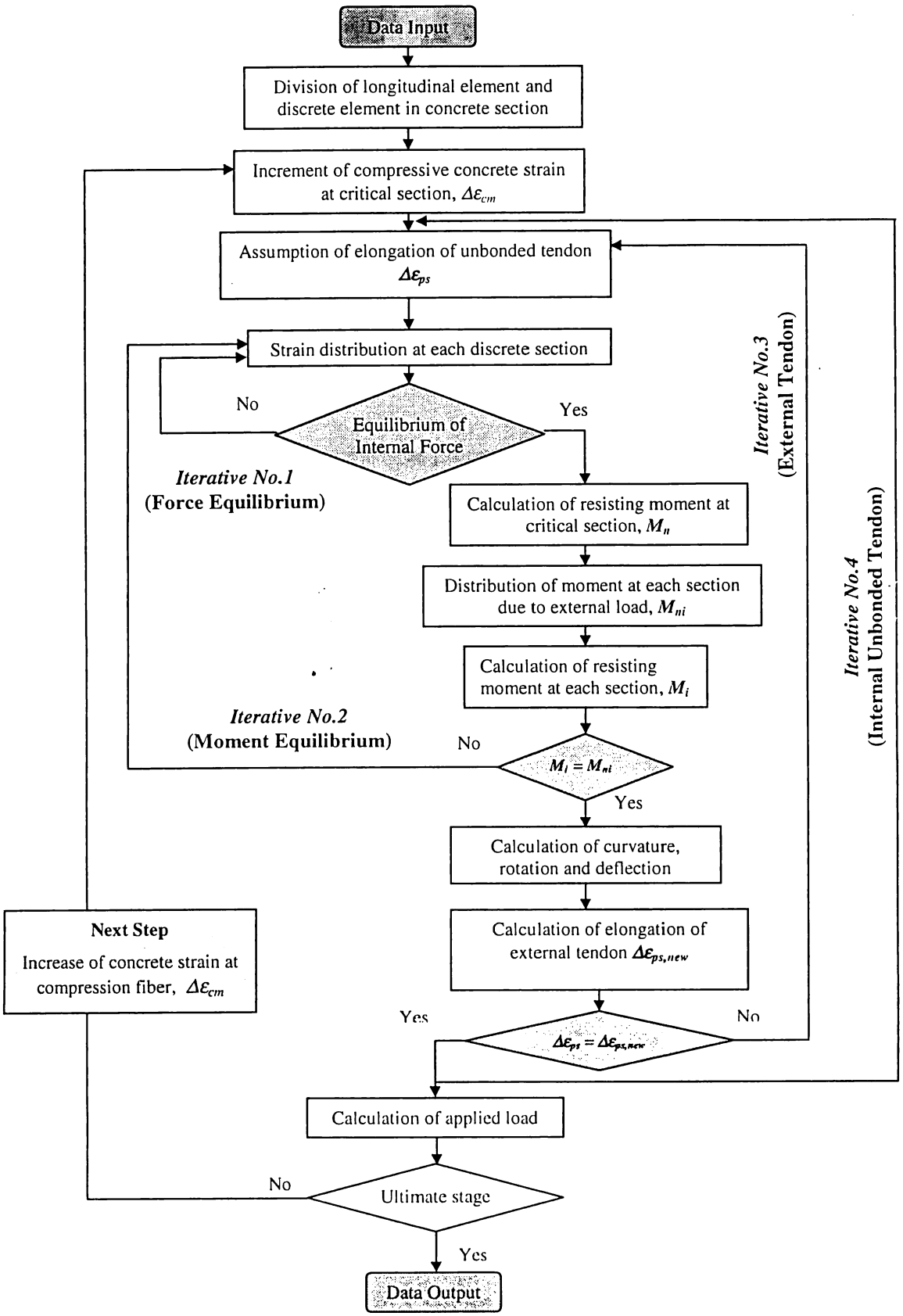


**Fig. 4-5 Flowchart of analytical program**

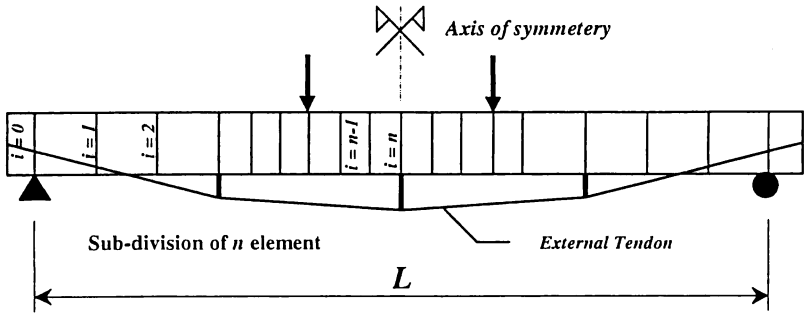


**Fig. 4-6 Analytical model of simply supported beam**

### (a) Initial stage

At the first step, from the input data such as properties of materials, dimensions of beam and the amount of prestressing force, the constant values involving the sectional properties, the constitutive model of material and so on were calculated. Next, the stress at top, $\sigma_t$, and bottom, $\sigma_b$, fiber of each discrete sections are calculated by assuming the elastic behavior of concrete section. This is because there is no crack occurs at this stage, hence, beam will behave like a homogeneous elastic material (Lin, T.Y. and et al., 1982 [23]). The step of calculation can be expressed as following equations.

$$\sigma_t = \frac{P_{ps}}{A_t} - \frac{(M_{ps} - M_d)y_c}{I} \tag{4-3}$$

$$\sigma_b = \frac{P_{ps}}{A_t} + \frac{(M_{ps} - M_d)(h - y_c)}{I} \tag{4-4}$$

where

$P_{ps}$ = the effective prestressing force

$A_t$ = the transformed area of transformed concrete section

$M_{ps}$ = moment due to prestressing force

$M_d$ = moment due to self weight of beam

$Y_c$ = neutral axis depth of transformed concrete section

$h$ = depth of concrete section

$I$ = moment of inertia of transformed concrete section

Then, the initial strain distribution at each discrete sections will be computed by using the nonlinear stress-strain relationship of concrete as given in Eq.4-1. Subsequently the

curvature, rotation and deflection at all integration points are determined by using the numerical integration method as usually used in moment-curvature analysis. This step was implemented until all of the initial values would be obtained involving the difference of internal force, the internal resisting moment and the concrete strain at all integration points which will be used in further step of analysis.

After obtaining the initial concrete strain at all discrete sections, the calculation is next proceeded by adding the strain at the extreme compression fiber of critical section, $\varepsilon_{cm}$, with the assumed increment $\Delta\varepsilon_{cm}$. Note that the critical section was firstly assumed to be at the mid-span section ($n$ integration point) in single span beam. The distribution of concrete strains at all integration points can be determined by considering the following three iterative loops.

**(b) Equilibrium of Internal Force (1st Iterative Loop)**

The internal forces of any discrete section comprising those from concrete, non-prestressed reinforcement and prestressing tendons, were calculated by dividing the concrete section into small fibers parallel to the neutral axis and assuming that the concrete strain is linearly distributed over the depth of beam (Fig. 4-1). The internal force of concrete of each fiber area can be determined by firstly computing the concrete strain at any level $i$ by using linear strain distribution and then changing such concrete strains to the corresponding stress by using the stress-strain relationship of concrete, and finally multiplying with the concrete area of each fiber to obtain the force. By summation of the concrete force at all $m$ discrete fibers, the total compressive force of concrete section can be obtained as given by following equations.

$$\begin{aligned} \varepsilon_c(i) &= \varepsilon_t - [(\varepsilon_t - \varepsilon_b)(i - 0.5)/m] \\ C &= \sum_{i=0}^{m} \sigma_c(i) b \Delta x \end{aligned} \qquad \text{(4-5)}$$

in which:

$C$ = summation of concrete force in section

$i$ = number of discrete element from the extreme top fiber

$\sigma_c(i)$ = concrete stress at level $i$ corresponding to concrete strain $\varepsilon_c(i)$

m = total number of horizontal discrete element

$\Delta x$ = h / m

In similar way, the tensile forces of non-prestressed reinforcements and internal bonded tendons can be evaluated. It should be noted that an assumption of perfect bond between steel reinforcements and surrounding concrete was adopted in such a way that the increased steel strain can be directly calculated from the concrete strain distribution on beam section. The method of calculations are given in following equations.

$$\begin{aligned} \varepsilon_{si} &= \varepsilon_t + (\varepsilon_b - \varepsilon_t)\frac{d_{si}}{h} \\ \Delta\varepsilon_{ps} &= \varepsilon_t + (\varepsilon_b - \varepsilon_t)\frac{d_{ps}}{h} \\ T_s &= \sum_{i=1}^{k} f_{si} A_{si} \\ T_{ps} &= f_{ps} A_{ps} \; ; \; f_{ps} = f_{pi} + \Delta f_{ps} \end{aligned} \tag{4-6}$$

in which:

$\varepsilon_{si}$ = strain of reinforcements at level $i$

$\Delta\varepsilon_{ps}$ = strain increase of internal bonded tendon

$T_s$ = total force of reinforcements

$f_{pi}$ = initial stress in internal bonded tendon

$\Delta f_{ps}$ = stress increase in internal bonded tendon corresponding to $\Delta\varepsilon_{ps}$

$T_{ps}$ = force in internal bonded tendon

As previously mentioned, force in unbonded tendons are initially assumed at the first step of calculation. Hence, at this step, a force equilibrium condition can be checked by summing the total internal forces which would give a zero value if the strain distribution of concrete is correctly estimated. If it is not so, the adjustment is made to the tensile concrete strain until the error in calculation is less than the allowable value defined in this study as 1% of total tensile force. After satisfying this condition at all integration points, the calculation is proceeded to the next step which is equilibrium of moment.

### (c) Equilibrium of Moment (2nd Iterative Loop)

The required condition in this step of calculation is that the magnitude of internal resisting moment should be equal to the applied moment caused by external load at all integration points. The total internal resisting moments at any section are comprised of those from concrete, reinforcements, internal tendon and external tendons. These internal moments were calculated by multiplying the force in each materials with the depths from the top fiber of concrete section, rather than the neutral axis. This is because it can reduce the difficulty in determining the neutral axis which will be changed as load was increased. The expression of calculation can be given as following equation.

$$M_i = M_{ci} + M_{si} + M_{psi} \tag{4-7}$$

in which:

$M_i$ = internal resisting moment at section $i$

$M_{ci}$ = moment due to concrete force at section $i$

$M_{si}$ = moment due to reinforcements at section $i$

$M_{psi}$ = moment due to prestressing force at section $i$

In this step, based on the concrete strains obtained in the first iterative loop, the internal resisting moment was first calculated at the critical section, $M_n$. By using this value along with the elastic analysis, the distribution of moment due to external load at any integration point, $M_{ni}$, can be determined. The criteria condition used in this study is that the difference between $M_i$ and $M_{ni}$ is less than the specified allowable error. If not so, an adjustment will be made to the compressive concrete strain, $\varepsilon_{ci}$, and the calculation will be re-started since the first iterative loop until the difference is less than the allowable tolerance for all integration points.

### (d) Compatibility Condition of Unbonded Tendon (3rd Iterative Loop)

After satisfying the calculation of force and moment equilibrium conditions, the strains in concrete at unbonded tendon level were numerically integrated to obtain the total deformation, $\delta_{cf}$. By deducing with the deformation of concrete at tendon level at initial

stage (before loading), $\delta_{ci}$, and divided by the entire length of unbonded tendon, the average strain increase of concrete at tendon level, $\Delta\varepsilon_{c,ps}$, can be obtained. Based on the *deformation compatibility*, this value should be equal to the average strain increase in unbonded tendon, $\Delta\varepsilon_{ps}$, which was initially assumed at the beginning of calculation (see Fig. 4-5). Therefore, in this step, the last criteria can be checked by comparing the assumed value of strain increase in tendon, $\Delta\varepsilon_{ps}$, with the new value calculated based on the deformation of concrete at tendon level, $\Delta\varepsilon_{ps,new}$ (or $\Delta\varepsilon_{c,ps}$). The allowable iterative error used in this study was specified as 1% of $\Delta\varepsilon_{ps,new}$. If this criteria is not obtained, the new assumed strain increase in unbonded tendon will be made and the preceding procedures involving force and moment equilibrium loop will be repeated until the difference of $|\Delta\varepsilon_{ps,new}-\Delta\varepsilon_{ps}|$ is within a specified value equal to 1% of $\Delta\varepsilon_{ps,new}$.

**(e) Failure Criteria**

After all three iterative loops are satisfied, the calculation of externally applied load was carried out by using the internal resisting moment at the critical section to determine the corresponding value of external load. This is based on the elastic theory as previously explained in the iterative loop of moment equilibrium. Subsequently, the computation was proceeded to the next loading step by increasing the compressive concrete strain at the critical section, $\varepsilon_{cm}$, and all the steps of calculation will be implemented again. It is important to be noted that the failure criteria defined in this analytical program can be summarized as follows: 1) concrete strain reach maximum compressive strain, 2) strains in reinforcements are larger than the ultimate strain of reinforcements, and 3) strains in prestressing tendons exceed the ultimate strain of tendons. When one of these failure modes is detected in the computation, the program will be terminated and the results can be seen in the output files.

### 4.3.4 Modification For Precast Segmental Beams

It has been investigated by a previous research (J. Muller and Y. Gauthier, 1989[24]) showing that the overall flexural behavior of precast segmental beams is mainly dependent on the behavior of joint opening. According to Fig. 4-7 which illustrates the behavior of

joint opening, it can be seen that the magnitude of joint rotation can be considered as the curvature at that joint section, $\phi_w$, because it is assumed that there is no bending within the segments. Also the depth of the contact surface, $h_c$, can be equivalent to the depth of neutral axis as used in the previous analytical method for monolithic beams. As a result, the precast segmental beams can be modeled in such a way that the integration points are selected at the segment joints because cracking can occur at these locations. In the step of calculating internal forces, the assumption that joint surface still remains plane after the occurrence of joint opening was adopted. This also implies that the strain distribution along the depth of beam is a linear distribution as shown in Fig. 4-7. In the analytical method, the contribution of main reinforcements is neglected as there is no continuity across segment joints.

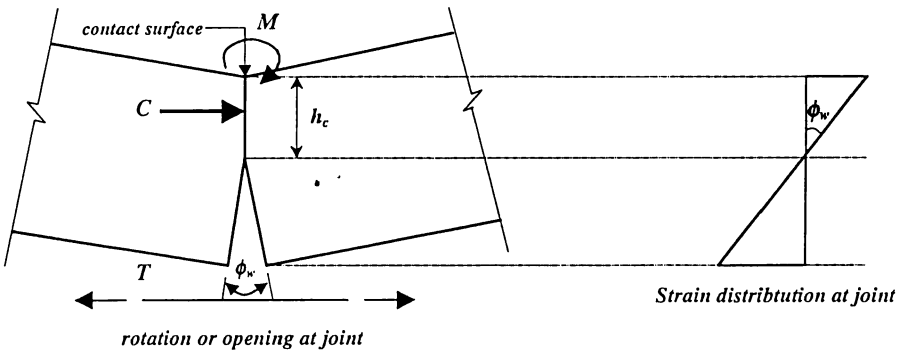


**Fig. 4-7 Joint opening behavior in precast segmental beam**

However, it was observed from the test results that after cracks or joint opening reached the mid-depth of concrete section, they tended to incline to the concrete sections under loading point which had maximum moment (see Appendix, photo 7). This clearly showed that the assumption of no bending within segment cannot be maintained anymore. This characteristics may be caused by the geometrical shape of precast segments used in the tests which had a ratio of width (312.5 mm) to depth (150 mm) around 2.08. In general precast segments, it yields value approximately 1.00, indicating a square-shaped block. To take into account of this characteristic, an assumption was made that the integration points can also be selected at the position inside the precast segment.

### 4.3.5 Modification for Internal Unbonded and External Tendons

The analysis of EPC beam with internal unbonded tendon provides additional difficulty as the stress increase in both prestressing tendons which is member-dependent characteristic has to be taken into account at the same time. In this study, a modification was made in the analytical program by adding an additional iterative loop for checking the compatibility of internal unbonded tendon after all three iterative loops as previously described are satisfied (Fig. 4-5). It should be noted that the assumption adopted for this computation is that the strain in internal unbonded tendon is uniformly distributed along its entire length. The computation of all iterative loops will be carried out until the required condition is obtained which is specified as $|\Delta\varepsilon_{ps,new}-\Delta\varepsilon_{ps}|_{int} \leq 0.5$ % of $(\Delta\varepsilon_{ps,new})_{int}$.

### 4.3.6 Geometrical Compatibility of External Tendon

As previously stated, some questions may be raised for the applicability of the concept of compatibility of deformation to the analysis of EPC beam with large eccentricities because it is apparent that a major portion of external tendon is placed considerably far from the concrete section, therefore, an additional assumption considering the imaginary concrete at tendon level has to be assumed (see Fig.4-1).

Another method to evaluate stress increase in external tendon has been proposed by Virlogeux, 1988 [9] by considering that, because of the rectilinear shape of external tendon between end anchorages, the elongation of tendon between deviations can be calculated providing the beams remain uncracked and linear elastic. This method is considered to be more realistic than the previous concept because it is based on the change of the geometry of external tendon as load was increased and is rather easy to visualize how the stress in external tendon can be increased at any stage of loading. This concept can be referred as "*the geometrical compatibility of external tendon*". To the best of author's knowledge, this method could be further extended even when after the occurrence of cracking, nonlinear behavior, provided that the deformations of beam at the deviations and anchorages can be accurately calculated up to the ultimate stage.

This statement can be preliminarily verified by means of calculating force in external tendon using the deflections of beam at all deviators measured in the tests. By knowing the deflections at any stage of loading, the deflected shape of external tendon can be determined, consequently, the elongation, $\Delta L$, and the strain increase, $\Delta\varepsilon_{ps}$, in external tendon could be also evaluated. Then the stress corresponding to such strain increase in external tendon was computed by using the stress-strain relationship as given in Eq.4-2. The comparisons of the calculated value with the experimental results of single span beams are shown in Fig. 4-8. It can be observed that by using such a simplified calculation, force in external tendon can be predicted with a reasonable accuracy up to the ultimate stage. This clearly indicates that the difficulty in evaluating force in external tendon can be coped with by considering only the deformations of beam at deviators in the structure.

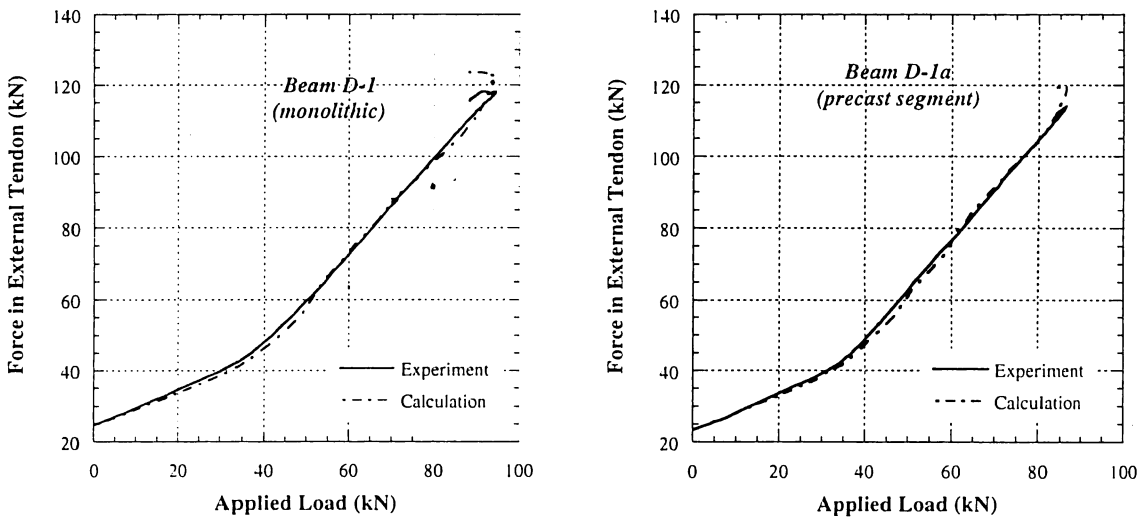


**(a) Beam D-1 (monolithic)** **(b) Beam D-1a (segmental)**

**Fig. 4-8 Comparison between external tendon force from simplified calculation and experimental results**

The application of this concept, *geometrical compatibility of external tendon*, to the analytical methodology can be described by using the analytical model of simply supported EPC beam with three deviators (Fig. 4-9). The assumption adopted for using this concept is that the strut deviator is considered as a rigid member implying that there is no relative deformation at the connection between concrete beam and deviators. In addition, the strain in external tendon is assumed to be uniformly distributed over the entire length of beam.

Therefore, we can calculate the elongation of external tendon, $\Delta L$, directly from the known deformations (rotation, $\theta$ and deflection, $\delta$) at deviators and, subsequently, strain increase in external tendon, $\Delta\varepsilon_{ps}$. In the analytical program, this calculation was implemented in the 3rd iterative loop for determining the strain increase in external tendon instead of using the compatibility of deformation.

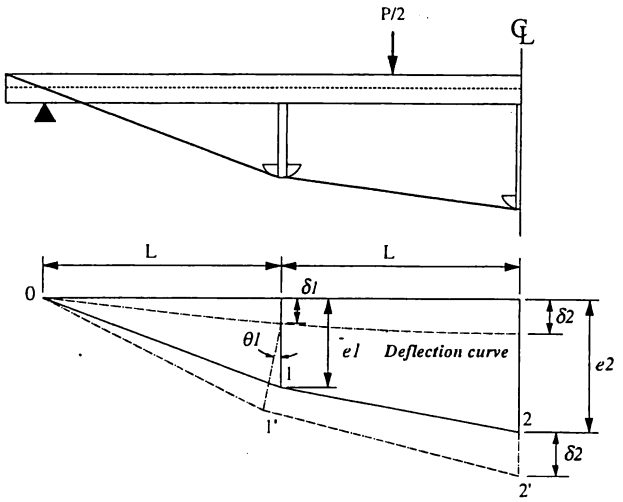


**Fig. 4-9 Deflected shape of simply supported beam under loading**

The step of calculation using concept of geometrical compatibility of external tendon can be expressed as following equations.

- Initial elongation of tendon, $L_i$

$$\begin{aligned} L_{01} &= \sqrt{L^2 + e_1^2} \\ L_{12} &= \sqrt{L^2 + (e_2 - e_1)^2} \\ L_i &= L_{01} + L_{12} \end{aligned} \tag{4-8}$$

- Final elongation of tendon, $L_f$

$$\begin{aligned} L_{01'} &= \sqrt{(L_{01'})_x^2 + (L_{01'})_y^2} \\ &= \sqrt{(L - e_1 \sin\theta_1)^2 + (\delta_1 + e_1 \cos\theta_1)^2} \\ L_{1'2'} &= \sqrt{(L_{1'2'})_x^2 + (L_{1'2'})_y^2} \\ &= \sqrt{(L + e_1 \sin\theta_1)^2 + (\delta_2 - \delta_1 - e_1 \cos\theta_1)^2} \\ L_f &= L_{01'} + L_{1'2'} \end{aligned} \tag{4-9}$$

- Strain increase in external tendon, $\Delta\varepsilon_{ps}$

$$\begin{aligned} \Delta L &= (L_{01'} + L_{1'2'}) - (L_{01} + L_{12}) \\ \Delta\varepsilon_{ps} &= \frac{\Delta L}{L_i} \end{aligned} \tag{4-10}$$

$e_1$, $e_2$ = eccentricity of external tendon at deviator 1 and 2

$\theta_1$, $\theta_2$ = rotations of beam at deviator 1 and 2

$\delta_1$, $\delta_2$ = deflection of beam at deviator 1 and 2

### 4.3.7 Comparison with Experimental Results (Single span beams)

A comparison between analytical predictions based on both deformation compatibility and geometrical compatibility of external tendon and experimental results is summarized in Table 4-1. Unexpectedly, it can be seen that the analytical predictions from both compatibility concepts showed nearly the same value of the ultimate load, deflection and force in external tendon. This finding implies that there may be a similarity in the fundamental concept of each method which will be further discussed in section 4.3.8. Of greater importance, by comparing with the experimental results, it can be observed that the predicted ultimate load was slightly lower than the test results of monolithic beam but little higher in case of precast segmental beam. This can be attributed to the imperfection of analytical program to simulate the behavior at joint in precast segmental beam in which a concentration of compressive strain can occur and resulting in early failure. Another interesting point should be given here is that the predicted value of ultimate deflection is considerably less than that of the test results. The magnitudes of such errors are approximately 20% and 27% for monolithic and precast segmental beam respectively. This difference may be caused by the fact that the calculation of deflection in the analytical program was based on the assumption of pure bending (moment-curvature method) in which the influence of shear deformation is neglected.

**Table 4-1 Comparison with experimental results (single span beam)**

| No. | Description | Ultimate Load (kN) | | | Ultimate Deflection (mm) | | | Ultimate External Tendon Force (kN) | | |
|---|---|---|---|---|---|---|---|---|---|---|
| | | Exp*1 | Def | Geo | Exp | Def | Geo | Exp | Def | Geo |
| D-1 | Monolithic | 94.5 | 92.9 (0.983)*2 | 93.2 (0.986) | 117.9 | 94.2 (0.799) | 96.4 (0.818) | 118.1 | 120.4 (1.019) | 120.5 (1.020) |
| D-1a | Precast segment | 86.3 | 86.7 (1.005) | 87.2 (1.010) | 100.2 | 72.8 (0.727) | 74.3 (0.742) | 114.3 | 113.5 (0.993) | 113.8 (0.996) |

**Note** *1 Exp: experiment, Def: deformation compatibility, Geo: geometrical compatibility of external tendon

*2 correlation ratio (Analysis/Experiment)

In case of beam D-1a which was provided with both external tendon and internal unbonded tendon, the relationship between increase of tendon force and applied load is shown in Fig. 4-10. It can be seen that force in internal unbonded tendon was nearly constant before the occurrence of first cracking corresponding to the load value of 37 kN. After cracking, forces in both external and internal tendon increased very rapidly compared to the previous stage. This is because the deflection of beam also increased at a high rate after cracking, resulting in large tendon elongation and consequently tensile stress in both internal unbonded and external tendon. By comparing the analytical results with those observed in the tests, it can be seen that a good agreement was obtained.

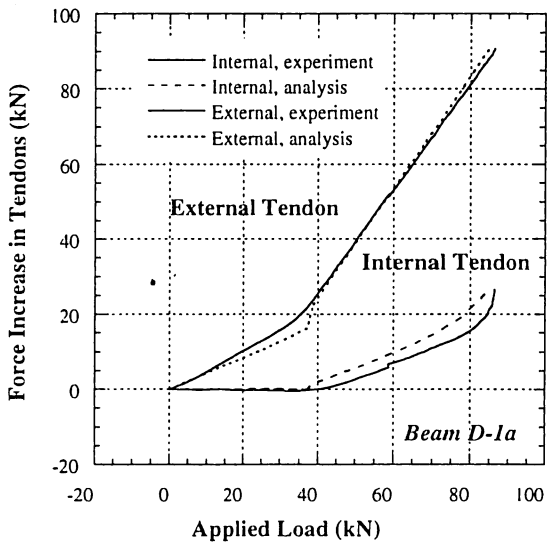


**Fig. 4-10 Force increase in prestressing tendons in beam D-1a (precast segment)**

Fig. 4-11 (a) and (b) show the comparative plots of load versus mid-span deflection and load versus force in external tendon obtained from the analytical program and experimental results. It can be seen that the predicted values of initial camber were somewhat less than the experimental results in both two beams. Notwithstanding, by considering the overall behavior of load-deflection or load-force in external tendon response, it can be concluded that the flexural analysis of EPC simply supported beams with large eccentricities can be predicted with a reasonable accuracy by using such an analytical methodology based on both two compatibility concepts.

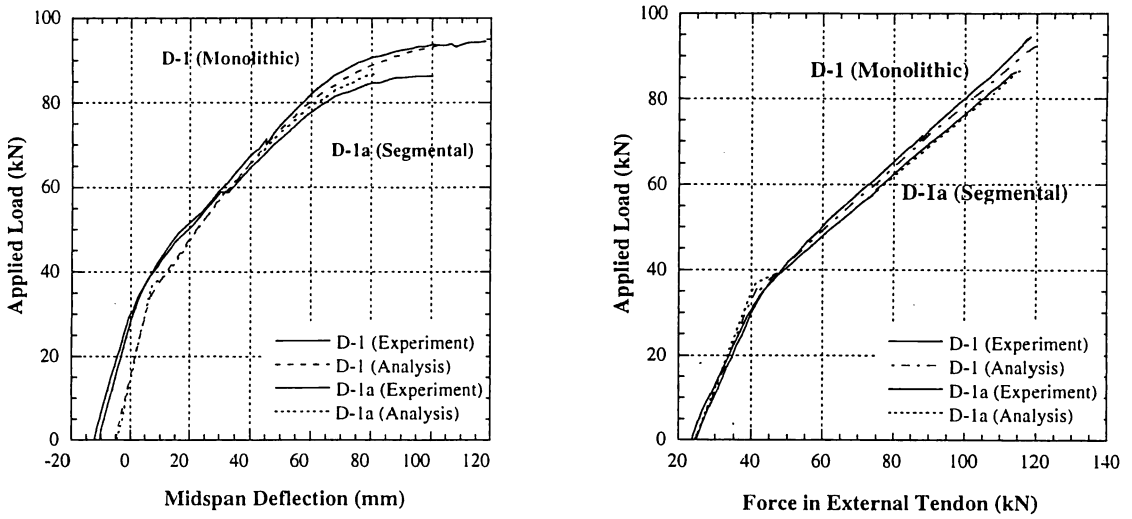


**(a) Load and mid-span deflection curve**

**(b) Load and force in external tendon relationship**

**Fig. 4-11 Comparison with experimental results of single span beams**

### 4.3.8 Verification of the Compatibility Concept of External Tendon

In previous section, it can be concluded that the analytical results using both compatibility concepts—*deformation compatibility* and *geometrical compatibility of external tendon*—showed almost nearly the same values and also agreed well with the experimental results.

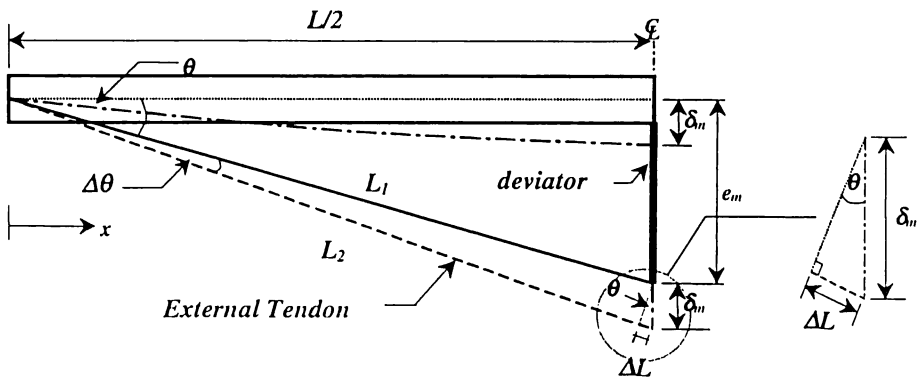


**Fig. 4-12 Model of simply supported beam**

For further investigation of the applicability of those concepts, an analytical study was carried out by using a model of EPC beam with large eccentricities as shown in Fig. 4-12. The model consists of a simply supported beam with a draped external tendon at mid-span section by strut deviator having eccentricity of $e_m$. The elongation of external tendon, $\Delta L$, was then calculated by using both compatibility concepts which can be described as below.

**(a) Compatibility of Deformation**

*Concept*:

- The concrete strain is assumed to be linearly distributed throughout the total depth of structure from the top fiber of concrete beam to the level of external tendon. Note that the concrete strain below the concrete section is assumed to be fictitious.
- The elongation of external tendon is calculated assuming to be equal to the total elongation of concrete at tendon level.

The unit strain in concrete at any point is given by;

$$\varepsilon = \frac{\sigma}{E_c} = \frac{My}{E_c I} \tag{4-11}$$

The total strain along the external tendon is then;

$$\begin{aligned} \Delta L &= \int_0^{L/2} \varepsilon dx \\ &= \int_0^{L/2} \frac{M(x)e(x)}{IE_c} dx \quad \text{in which } e(x) = x\frac{e_m}{L/2} \\ &= \int_0^{L/2} \phi(x)e(x)dx \end{aligned} \tag{4-12}$$

Hence,

$$\Delta L = \frac{e_m}{L/2} \int_0^{L/2} x\phi(x)dx \tag{4-13}$$

Solve Eq.4-13 by using method of integration by part;

$$\begin{aligned} &\int udv = uv - \int vdu \\ &u = x \;\; ; \; dv = \phi(x)dx \\ &du = dx \; ; \; v = \int \phi(x)dx = \theta(x) \end{aligned} \tag{4-14}$$

Hence, we can obtain;

$$\begin{aligned}\int_0^{L/2} x\phi(x)dx &= uv - \int vdu \\ &= \left[x\theta(x) - \int \theta(x)dx\right]_0^{L/2} \\ &= -\int_0^{L/2} \theta(x)dx = \int_{L/2}^{0} \theta(x)dx\end{aligned} \tag{4-15}$$

Therefore, Eq.4-13 can be rewritten as following;

$$\begin{aligned}\Delta L &= \frac{e_m}{L/2}\int_0^{L/2} x\phi(x)dx \\ &= \frac{e_m}{L/2}\int_{L/2}^{0} \theta(x)dx \\ &= \frac{e_m}{L/2}\delta_m\end{aligned} \tag{4-16}$$

**(b) Geometrical Compatibility of External Tendon**

*Concept*:

- The concrete strain is assumed to be linearly distributed throughout the depth of concrete beam section.
- The elongation of external tendon is determined by considering the change of shape of external tendon as load is increased.

From Fig.4-13, we can obtain;

$$\begin{aligned}\Delta L &= L_2 - L_1 \\ &\approx \delta_m \sin\theta \quad ; \Delta\theta \approx 0 \\ &\approx \delta_m \tan\theta \quad ; \theta \approx 0\end{aligned} \tag{4-17}$$

Substituting $\tan\theta = \frac{e_m}{L/2}$ into Eq.4-17;

$$\Delta L = \frac{e_m}{L/2}\delta_m \quad \text{(Same as Eq.4-16)} \tag{4-18}$$

It can be observed from Eq.4-16 and Eq.4-18 that both compatibility concepts showed the same value of elongation of external tendon, implying that they are basically based on the same fundamental concept. In addition, it is apparent that elongation of external tendon,

$\Delta L$, is a function of the mid-span deflection, $\delta_m$, and its geometrical shape, $\tan\theta$. Hence, it can be concluded that force in external tendon is totally dependent on its geometrical shape and deformations of structure at deviators and anchorages. In case of internal unbonded tendon, deviators can be regarded existing along entire beam whereas, in external tendon, they will be only at the discrete number of deviators (Fig.4-13). This characteristic results in much more simplified calculation of force increase in external tendon as it can be directly determined from the change of geometrical shape unlike internal unbonded tendon in which the elongation of tendon has to be carried out by integration method which is the basis of deformation compatibility concept.

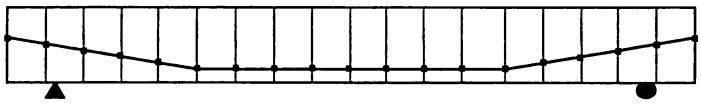

*Internal unbonded prestressing model*

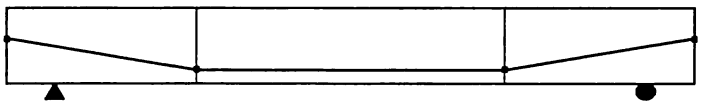

*External unbonded prestressing model*

**Fig. 4-13 Model of unbonded prestressed concrete**

Therefore, a conclusion can be drawn that both compatibility concepts are in nature the same methodology to calculate the elongation of unbonded tendon by considering the geometrical shape of tendon as well as the deformation at deviators and anchorages. These methods can be applied regardless how far the level of external tendon from the concrete section or, in other words, there exists the real concrete strain at tendon level or not. However, in case of EPC beams with large eccentricities, to obtain a clearer understanding of behavior of stress increase in tendon as well as to simplify the calculation, it is recommended that the geometrical compatibility of external tendon be used as a basis for evaluation of force in external tendon.

## 4.4 Modification for Two-Span Continuous Beams

In two-span continuous PC beams, it is generally known that the effect of secondary moment and moment redistribution occurred due to the geometrical condition of structure

at the center support in which the rotational capacity is prevented unlike in simply supported beams. These characteristics can have a marked influence on the flexural behavior of two-span continuous beams especially in the nonlinear response, therefore, some modifications are necessary which will be discussed as follows.

Moment due to prestressing, $M_p$, in two-span continuous beams is comprised of two components: primary moment, $M_{pri}$, and secondary moment, $M_{sec}$. The primary moment can be easily calculated by considering that there is no center support or like two simply supported beams and the calculation is carried out as in static determinate structure. Next, the real system of beam with center support was considered to be applied by such primary moment. The calculated internal moment at any section can be referred as the total moment due to prestressing, $M_p$. Finally, the secondary moment can be calculated by following equation:

$$M_{sec} = M_p + M_{pri} \tag{4-19}$$

Questions may be raised whether the secondary moment is appear at the ultimate limit state or not. To the best of author's knowledge, it will mainly depend on the rotational capacity of section at center support in case of two-span continuous beams. If the fixed condition at center support can not be maintained due to the occurrence of cracking or yielding of reinforcement the magnitude of secondary moment will tend to decrease. In this study, a modification of secondary moment was implemented by assuming that the reduction of secondary moment is equal to the magnitude of redistributed moment at the center support.

In order to evaluate the amount of moment redistribution, the model of moment-load relationship was proposed (Fig. 4-14). After yielding, which can be considered as the cracking at center support in this study, the bending moment diagram will differ from that determined by linear-elastic analysis. The negative moment at center support will increase much slower than in the previous step. In contrast, the positive moment at mid-span region or under loading point in this study will increase with a rate higher than that of center support. The relationships of these two rates of moment increase can be determined by assuming that the amount of redistributed moment at any section is linearly distributed

along beam length implying the same characteristic of secondary moment. At the ultimate stage, the moment at both critical sections will reach the ultimate moment, $M_u$, resulting in a collapse mechanism.

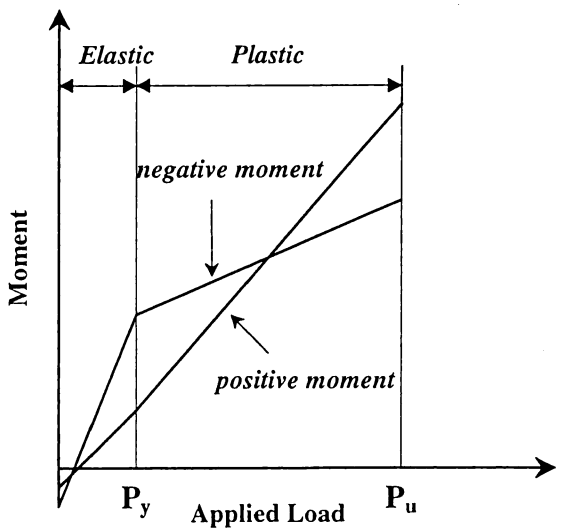


**Fig. 4-14 Model of moment versus applied load**

### 4.4.1 Comparison with Experimental Results (Two-span continuous beams)

A comparison between experimental versus analytical results of two-span continuous beams is summarized in Table 4-2. The comparative plots are also given in Fig.4-15 (a) and (b). It can be seen that there is a reasonable agreement between experimental and analytical results. However, it should be noted that the predicted values of ultimate deflection are considerably less than that of the test results, which are approximately 20% for both two specimens. This difference may be caused by the assumption used in the calculation of deflection in the program which considered only pure flexural deformation.

**Table 4-2 Comparison with experimental results (two-span continuous beams)**

| No. | Description | Ultimate Load (kN) | | | Ultimate Deflection (mm) | | | Ultimate Tendon Force (kN) | | |
|---|---|---|---|---|---|---|---|---|---|---|
| | | Test | Analysis | Correlation | Test | Analysis | Correlation | Test | Analysis | Correlation |
| A-1 | monolithic | 108.3 | 104.8 | 0.968 | 82.7 | 66.0 | 0.798 | 115.9 | 112.2 | 0.968 |
| A-1a | precast segment | 100.8 | 99.2 | 0.984 | 80.0 | 65.7 | 0.821 | 112.6 | 109.1 | 0.969 |

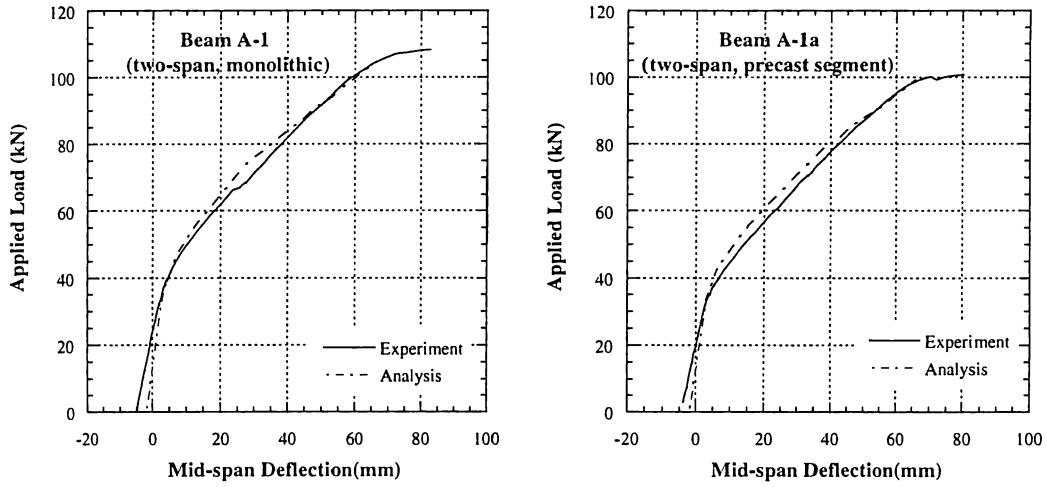


**(a) Load and mid-span deflection relationship**

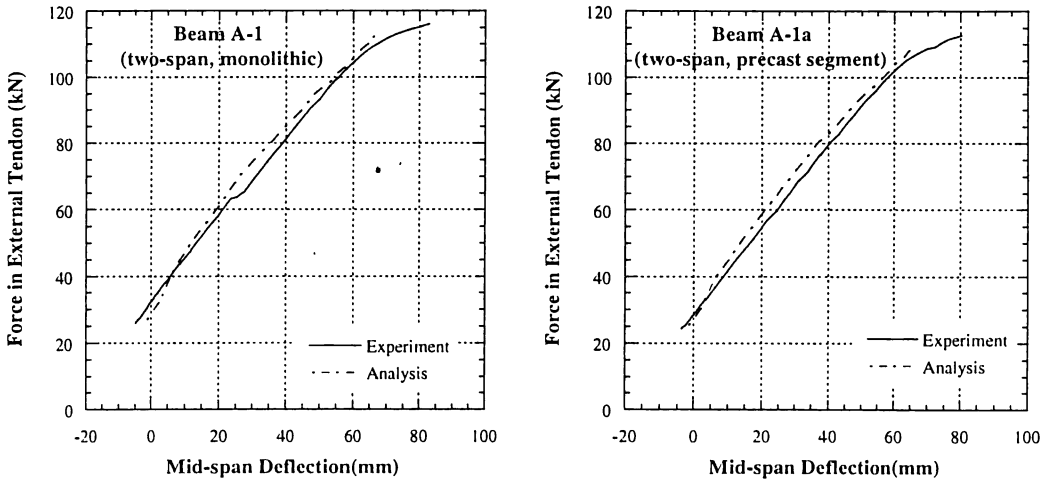


**(b) Force in external tendon and mid-span deflection relationship**

**Fig. 4-15 Comparison between experimental and analytical results of two-span continuous beams**

## 4.5 Conclusions

In this chapter, an analytical methodology for predicting the ultimate flexural strength of EPC beams with large eccentricities was discussed. The analytical program was based on the conventional moment-curvature method and the *compatibility of deformation* of external tendon. The assumption of imaginary concrete strain at tendon level in the concept

of deformation compatibility was discussed and theoretically verified to be applicable for using in the analysis of EPC beams with large eccentricities. This was carried out by comparing with a different concept, *geometrical compatibility of external tendons*, showing nearly the same value compared with those of the experimental results. The methodology was also extended to the analysis of two-span continuous beams by including the effect of secondary moment and moment redistribution. A good agreement between experimental results and analytical predictions was obtained. However, there still have some error in the predicted value of deflection in all test beams. This may be caused by the effect of shear deformation occurred in this type of structure especially at center support region in two-span continuous beams. A further research is recommended to include such an effect in the analytical methodology.

# CHAPTER 5

# Investigation of EPC Beams with Large Eccentricities under Shear-type Loading

## 5.1 Introduction

In recent years, questions have been raised about the shear behavior of PC beams with unboned or external tendons because it is apparent that there is no bond between prestressing tendons and surrounding concrete. Hence, the shear transfer mechanism of PC beam with external tendon might be different from those with internal bonded ones. Further, it can be observed that the investigations in this topic have been so far very little compared to those of flexural behavior especially in precast segmental beams. In order to obtain a better understanding of the shear behavior of EPC beam with large eccentricities, an experimental program was carried out in both monolithic and precast segmental beams with emphasis on the influence of stress increase in large eccentric external tendons.

## 5.2 Experimental Program

### 5.2.1 Overview

The main objectives of this experimental investigation were to investigate the structural behavior of EPC beams with large eccentricities under shear-type loading. At the beginning of test program, the beams were designed to obtain the shear failure by calculating shear strength according to JSCE [25] standard and flexural strength from the analytical program described in previous chapter. The safety factor defined as the ratio of flexure-failure load to shear-failure load was specified to be approximately 1.5. Various important parameters having influence on shear strength were selected including 1) method

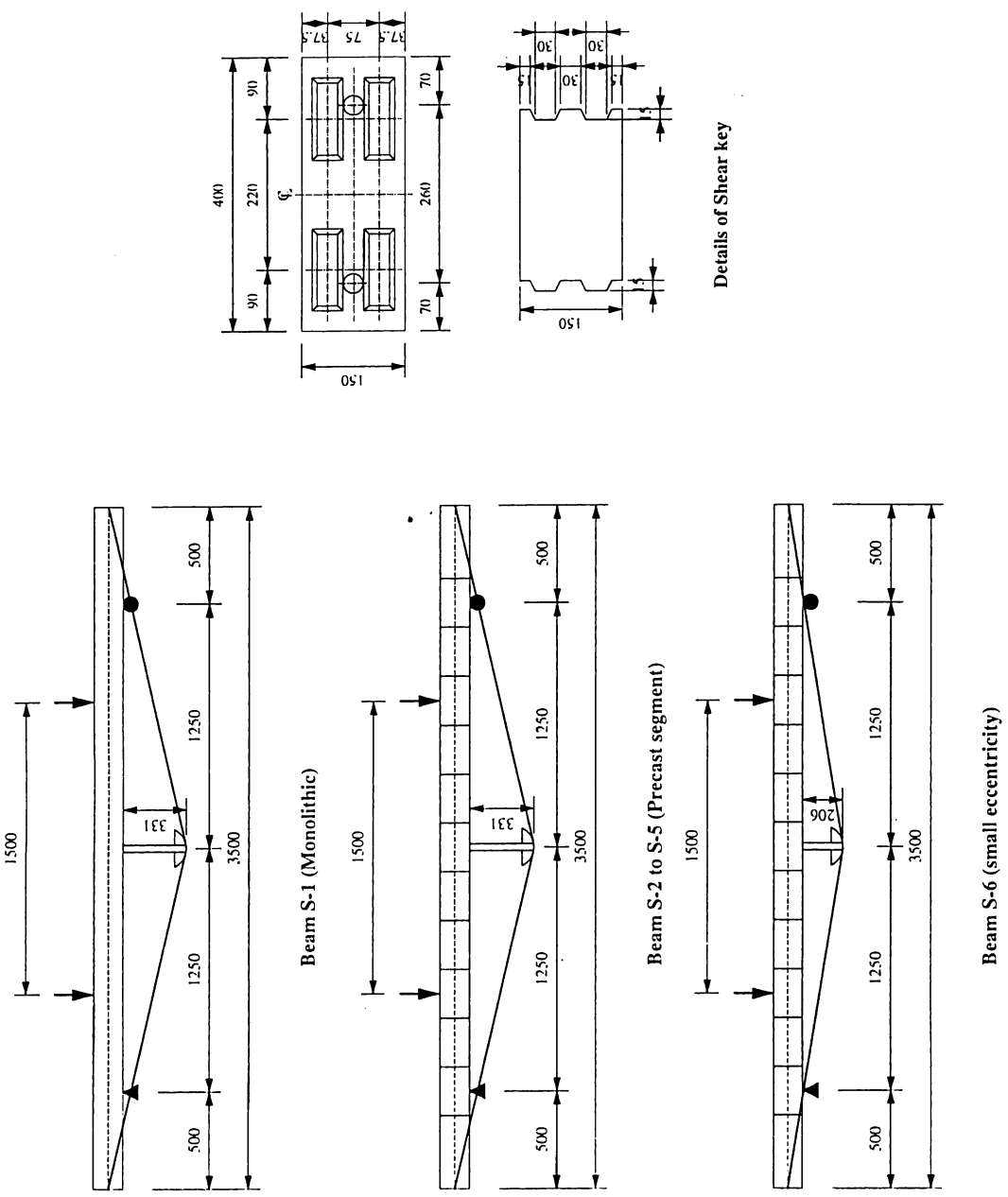


**Fig. 5-1 Layout of shear-type specimens**

of casting, 2) main reinforcement, 3) stirrup reinforcement, 4) eccentricity of external tendon, and 5) bonding condition of internal tendon. Nevertheless, after obtaining some test results indicating the flexural failure mode for first two specimens, it was decided to change the test parameter to the amount of initial prestressing forces both in internal and external tendons for the remaining specimens. This is because it was observed from the test results that the existence of compressive prestressing force and the vertical component of external tendon force substantially increased the shear strength of this type of structure. The details of test specimens and test variables are presented in following section.

### 5.2.2 Details of Specimens and Test Variables

Test specimens consisted of six simply supported beams with a rectangular-shaped cross section of 40 cm width and 15 cm height, the same dimension as flexure-test specimens. Table 5-1 shows the summary of test variables and material used in test. The details of mechanical material properties of reinforcements, prestressing tendons and epoxy can be found in chapter 2.

The layout of all test specimens is illustrated in Fig.5-1. All test beams were provided with two internal tendons of SWPR7B type with 12.4 mm diameter and one external tendons of SWPR19N type with a diameter of 21.8 mm. External tendons were deviated at mid-span section by a strut deviator, leading to a single-draped shape tendon. For internal tendons, they are of straight-lined tendons along beam length provided at the mid-depth level of concrete section. The utilization of internal tendons was primarily to prevent crack at the top fiber of concrete section due to the prestressing moment from external tendons at the initial stage as well as to provide an initial compressive force for assembling precast segments with epoxy resin in precast segmental beams. The concrete mix was designed for a 28-day compressive strength, $f_c'$, of 50 MPa. However, at the day of testing it was found that the concrete compressive strengths of all test beams were average of 70 MPa, fairly higher than the design value.

For precast segmental beams, each beam consists of 13 math cast segments with the width of 250 mm. They were assembled after applying epoxy resin at all shear-key surfaces by

introducing an initial compressive force of approximately 20 kN. After the initial required strength of epoxy was developed which took around 1 days according to the specification, internal tendons were then fully prestressed up to the design value. It should be noted that, before testing, it required at least 1 week for fully developed strength of epoxy resin.

**Table 5-1 Summary of test variables and material for shear-type specimens**

| No. | Method of Casting | Tendon Eccentricity (cm) | Reinforcement | | Prestressing Tendons | | Concrete Strength, $f_c'$ (MPa) |
|---|---|---|---|---|---|---|---|
| | | | Main | Stirrup | Internal | External | |
| S-1 | Monolithic | 40.6 | 4-DB6 | - | 2-T12.4 mm Unbond (100 kN) | 1-T21.8 mm (25 kN) | 75.9 |
| S-2 | Segmental epoxy joints | | - | - | 2-T12.4 mm Unbond (100 kN) | 1-T21.8 mm (25 kN) | 66.1 |
| S-3 | | | 4-DB6 | - | 2-T12.4 mm Bond (100 kN) | 1-T21.8 mm (25 kN) | 70.2 |
| S-4 | | | 4-DB6 | - | 2-T12.4 mm Bond (25 kN) | 1-T21.8 mm (10 kN) | 70.7 |
| S-5 | | | 4-DB6 | DB6@100 | - | 1-T21.8 mm (5 kN) | 70.2 |
| S-6 | | 28.1 | 4-DB6 | - | 2-T12.4 mm Unbond (25 kN) | 1-T21.8 mm (25 kN) | 66.3 |

### 5.2.3 Test Setup and Measurements

The beams were instrumented to measure the response of the structure to the applied load including concrete and steel strain, joint opening, force in prestressing tendons and deflections at mid-span and loading points. The details of such measuring devices can be found in chapter 2. All specimens were tested up to the ultimate by two-point static loading with a distance of 1.50 m, resulting in a shear span length of 0.5 m. The cracking load was recorded when the first crack or joint opening was observed. Test data was automatically recorded by the data logger in which the response of beam such as load-deflection curve can be monitored at the time of testing. It should be also noted tests of beam S-3 to 5 were carried out by removing the loading and support steel plates in order to provide the shear span length as the designed value.

## 5.3 Experimental Results and Discussions

The summary of experimental results of all shear-type specimens is shown in Table 5-2.

It can be seen that all test beams except beam S-2 were failed in flexure-type mode by compression of concrete at critical sections. It is important to note that beam S-3 was provided with internal bonded tendon but showed quite lower ultimate load than that of beam with internal bonded tendon (S-1). This may by caused by the fact that there was no loading steel plate in test of beam S-3, thus a concentration of compressive concrete strain can occurred at the region under loading point leading to an early failure mechanism.

**Table 5-2 Summary of experimental results of shear-test specimens**

| No. | Cracking Load (kN) | Ultimate Load (kN) | Prestressing Tendon Force (kN) | | | | Mid-span Deflection (mm) | | Mode of Failure |
|---|---|---|---|---|---|---|---|---|---|
| | | | Internal | | External | | Initial | Ultimate | |
| | | | Initial | Ultimate | Initial | Ultimate | | | |
| S-1 | 103.0 | 403.2 | 101. 9 | 143.5 | 21.8 | 290.8 | -2.77 | 27.36 | Crushing of concrete |
| S-2* | 107.9 | 265.9* | 100.5 | 122.5* | 23.2 | 191.9* | -5.09 | 16.56* | No failure |
| S-3 | 78.5 | 274.7 | 100.6 | 188.0 | 19.9 | 184.2 | -1.22 | 18.08 | Crushing of concrete |
| S-4 | 44.1 | 280.6 | 23.7 | 92.9 | 8.1 | 200.9 | -0.42 | 24.46 | |
| S-5 | 31.9 | 114.8 | - | - | 4.5 | 79.2 | -0.11 | 12.36 | |
| S-6 | 43.2 | 137.5 | 19.9 | 43.9 | 22.1 | 134.4 | -0.97 | 16.20 | |

*Note: test of beam S-2 was stopped when the compressive concrete strain at critical section reached the value of 2000 micron.

Crack patterns of shear-type specimens are illustrated in Fig. 5-2. Cracks first occurred at the regions near the loading points in monolithic beam or at the concrete adjacent to the critical joints in precast segmental beams and propagated rapidly until the crushing of concrete. It should be noted that there was only few large cracks occurred at the critical sections. This can be attributed to influence of resisting moment from external tendon which had a large magnitude in the loading span region, thus effectively preventing crack in such region to take place.

Fig. 5-3 shows a plot of load versus mid-span deflection of shear-type specimens. It can be seen that all test beams showed a bilinear curve with a deflected point at the occurrence of cracking. The difference of cracking loads in each test beam can be attributed to the amount of initial prestressing force which was lower in beam S-4 to 6.

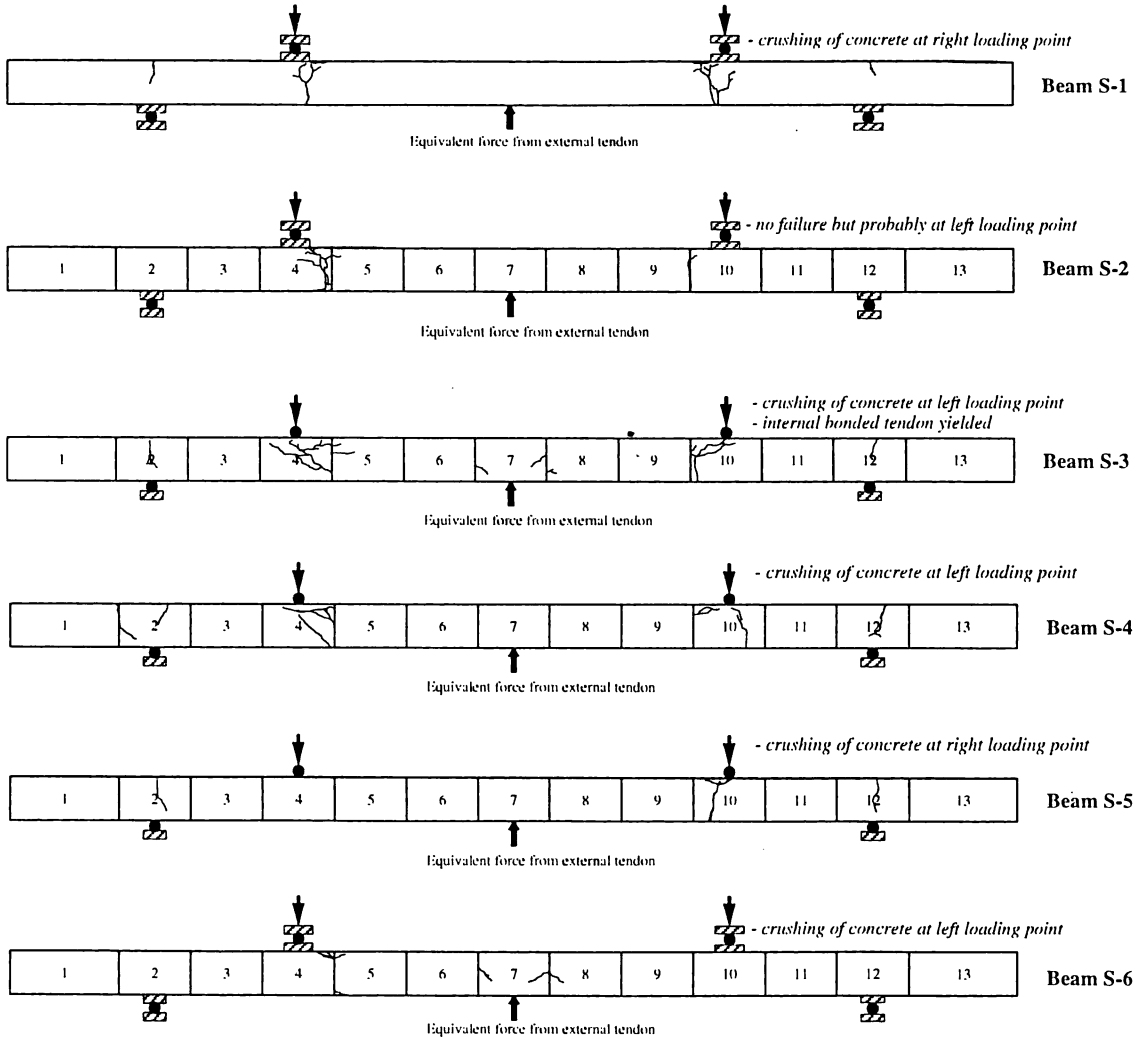


**Fig. 5-2 Crack patterns of shear-type specimens**

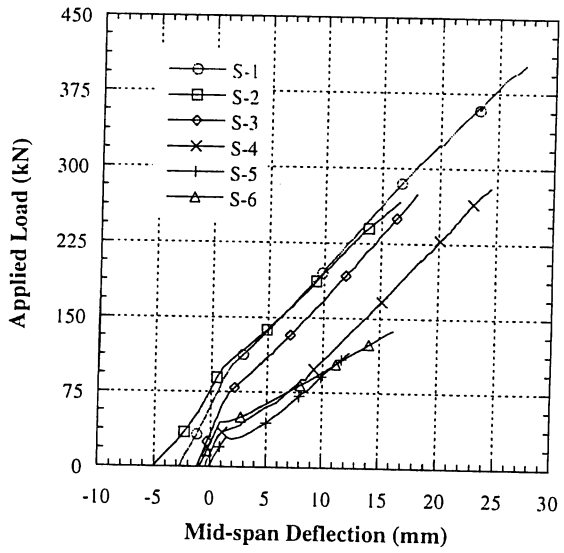


**Fig. 5-3 Load and mid-span deflection relationship of shear-type specimens**

The relationship of force in external tendons and mid-span deflection is plotted in Fig. 5-4. It can be observed that force in external tendons increased very rapidly after the occurrence of cracking. There was the same linear relationship in all test beams with a increasing rate of about 10 kN/mm except beam S-6 which had slightly lower value of 8.3 kN/m. This can be attributed to the different geometrical shape of external tendon whereby beam S-6 had a smaller eccentricity at mid-span section.

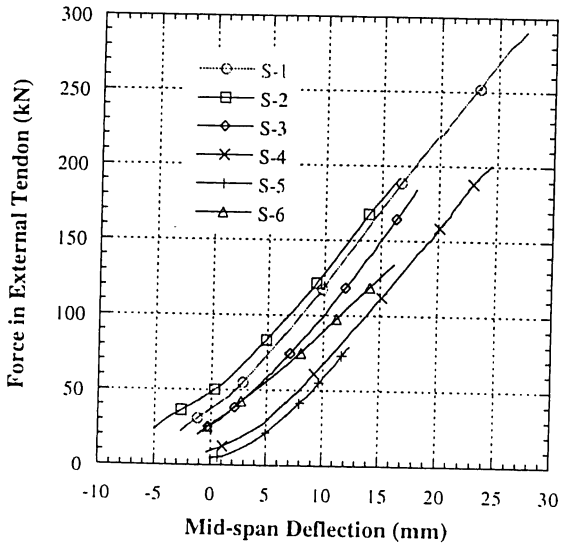


**Fig. 5-4 Force in external tendon of shear-type specimens**

## 5.4 Comparison with Shear Design Equation

To investigate the applicability of existing shear design equations for this type of structure, a comparison was made between the ultimate strength observed from tests which can be considered as the lower limit value of shear strength with those calculated based on JSCE and ACI code.

### JSCE Code [25]

The shear design equation is given as following equation:

$$V_{yd} = V_{cd} + V_{sd} + V_{ped} \tag{5-1}$$

$V_{cd}$ = design shear capacity carried by concrete

$$V_{cd} = f_{vcd} \cdot b_w \cdot d / \gamma_v$$

$$f_{vcd} = 0.9\beta_d \cdot \beta_p \cdot \beta_n \cdot \sqrt[3]{f_{cd}'}$$

$$\beta_d = \sqrt[4]{100/d}\ (d:cm) \qquad ;\text{when } \beta_d > 1.5, \beta_d \text{ is taken as } 1.5$$

$$\beta_p = \sqrt[3]{100\rho_w} \qquad ;\text{when } \beta_p > 1.5, \beta_p \text{ is taken as } 1.5$$

$$\beta_n = 1 + M_0/M_d \ (N'_d > 0) \qquad ;\text{when } \beta_n > 2.0, \beta_n \text{ is taken as } 2.0$$

$$= 1 + 2M_0/M_d \ (N'_d < 0) \qquad ;\text{when } \beta_n > 0, \beta_n \text{ is taken as } 0 \tag{5-2}$$

$$\gamma_b = 1.3 \text{ and } \rho_w = A_s / b_w d$$

$V_{sd}$ : design shear capacity carried by shear reinforcing steel

$$V_{sd} = [A_w f_{wyd} (\sin\alpha_s + \cos\alpha_s)/s_s]z/\gamma_b$$

$f_{wyd}$ : not greater than 4000 kgf/cm2 (5-3)

z = d/1.15 and $\gamma_b = 1.5$

$V_{ped}$ : component of effective tensile force of longitudinal tendon parallel to the shear force

$$V_{ped} = P_{ed} \sin\alpha_p / \gamma_b \ ; \ \gamma_b = 1.5 \tag{5-4}$$

### ACI 318-95 [20]

The shear design equation is given as following equation:

$$V_u = \phi(V_c + V_s)$$

$V_c$ : concrete shear strength (smaller value of $V_{ci}$ and $V_{cw}$)

$V_{ci}$ : Inclined shear cracking

$$V_{ci} = 0.6\sqrt{f'_c}\,b_{wd} + V_d + \frac{V_i M_{cr}}{M_{\max}} \tag{5-5}$$

$$M_{cr} = (I / y_t)(6\sqrt{f_c'} + f_{pe} - f_d) \tag{5-6}$$

$V_{cw}$ : web shear cracking

$$V_{cw} = (3.5\sqrt{f_c'} + 0.3 f_{pc})b_{wd} + V_p \tag{5-7}$$

$V_s$ : shear strength from shear reinforcement

$$V_s = \frac{A_v f_y d}{s} \tag{5-8}$$

**Table 5-3 Comparison with shear design equation**

| No. | Ultimate Shear Strength (kN) | | |
|---|---|---|---|
| | Test | JSCE | ACI |
| S-1 | > 403.2 | 73.6 | 88.7 |
| S-3 | > 274.7 | 73.8 | 84.3 |
| S-4 | > 280.6 | 58.5 | 67.3 |
| S-5 | > 114.8 | 100.6 | 100.1 |
| S-6 | > 137.5 | 73.1 | 75.0 |

From Table 5-3, it can be seen that the ultimate shear strength from both JSCE and ACI code showed conservative value compared with the lower limit value of assumed shear strength from the test. It is interesting to note that, in beam S-5, in which the amount of prestressing force is smallest and the stirrup is provided, the discrepancy was found to be very least compared to other beams.

## 5.5 Conclusions

An investigation of behavior of EPC beams with large eccentricities under shear-type loading was carried out. It was found that the ultimate shear strength of EPC beams with large eccentricities was very high due to the large magnitude of large eccentric external tendon force and the existence of compressive stress at the ultimate. This clearly indicated that the application of external prestressing can be effectively utilized not only for enhancing the ultimate flexural strength but also the shear strength of structure. In addition, it was found that shear strength from JSCE and ACI standard showed very conservative values for predicting the ultimate shear strength of EPC structure with large eccentricities.

# CHAPTER 6

# Conclusions

## 6.1 Conclusions

It has been generally known that in recent years the application of external prestressing is becoming more popular and widely used for modern bridge structures. Very recently, the concept was also developed in order to improve the flexural strength by placing external tendon outside the concrete girder at large eccentricities. It has been found that an effective utilization of external tendon as a tension member and concrete section as a compression one could be obtained resulting in a substantial enhancement of the ultimate flexural strength. However, to the best of author's knowledge, a clear understanding of the flexural behavior of this innovative type of structure has not yet been clarified regarding the ultimate flexural strength and force increase in external tendons especially in precast segmental beams. Further, the investigations of shear behavior of EPC beams with large eccentricities, which is also an important design aspect, have been so far very few. As a result, a study on both flexural and shear behavior of this type of structure was carried out in this study.

In order to obtain a better understanding of the flexural behavior of EPC beams with large eccentricities, an experimental program was conducted in both single span and two-span continuous beams. The results have shown that the flexural behavior of both monolithic and precast segmental beams was nearly the same at any stage of loading. This is because there was no main reinforcement in monolithic beams, thus showing the overall behavior nearly same as in precast segmental beams. In addition, the effect of internal unbonded tendon was also investigated in single span beam with an emphasis on the ultimate flexural strength and the ductility of structure. This kind of a mixed prestressing method may be preferred in the precast segmental construction because the problem of the quality of

grouting concrete can be eliminated, resulting in a better durability of bridge structure. It was found that the provision of external and internal unbonded tendons in precast segmental beam showed slightly lower ultimate flexural strength and ductility compared to those with internal bonded tendon. Such effects, however, were considered to be insignificant. This is because most of flexural strength was mainly from the large eccentric external tendons.

A nonlinear analytical methodology based on moment-curvature method and deformation compatibility was adopted in this study for analyzing the flexural behavior of EPC beams with large eccentricities. The assumption of imaginary concrete was theoretically verified by using a different analytical methodology base on the concept of geometrical condition of external tendon. The conclusion can be drawn that both analytical method are fundamentally the same methodology to calculate the elongation of unbonded tendon by considering the geometrical shape of tendon and the deformation of structure at deviators and anchorages. These methods can be accurately utilized regardless of the eccentricity of external tendon provided that the inclined concrete strain component at tendon level can be assumed to be insignificant. Nevertheless, in the analysis of EPC beams with large eccentricities, to obtain a better understanding of the mechanism of stress increase in tendon, it is recommended that the geometrical compatibility of external tendon be used as a basis for evaluation of stress in large eccentric external tendon.

In respect of the shear behavior of EPC beam with large eccentricities, an experimental program was conducted in both monolithic and precast segmental beams with emphasis on the influence of stress increase in large eccentric external tendons. Notwithstanding, it was found that the shear strength of this type of structure was comparatively high and all the test specimens failed in flexure-type. This is because external tendon force can be increased rapidly as load was increased, therefore, the contribution to shear strength from the vertical component of external tendon force is very large particularly at the ultimate stage compared to those of conventional EPC beams. In addition, it was also found that shear strength from JSCE and ACI standard showed very conservative values for predicting the ultimate shear strength of EPC structure with large eccentricities.

## 6.2 Recommendation for Further Study

It can be concluded from this study that the ultimate flexural strength can be predicted with a good accuracy by using the developed analytical program. However, there still have some erratic parts in such a program as it can be seen that the predicted value of the ultimate deflection was very lower than observed value from test around 20%. This is believed to be caused by the effect of shear force on this kind of structure particularly at the center support region in two-span continuous beam. Therefore, a modification is recommended to take into account such an effect of shear deformation. Further, in the analysis of two-span continuous EPC beam with large eccentricities, there still have some difficulties to predict the magnitude of redistributed moment at the ultimate stage as well as the reduction of the secondary moment. Some parameter affecting such a behavior should be further investigated in order to obtain an accurate model. Finally, even though it can be concluded from the current study that EPC beam with large eccentricities will not have much problem under shear-type loading, a further investigation is recommended in order to obtain an accurate prediction of the shear strength of this kind of structure, especially the influence of the absence of bonding between prestressing tendons and surrounding concrete.

# REFERENCES


[1] Beaupre R.J., Powell, L.C., Breen, J.E., and Kreger, M.E. (1989). *"Deviator Behavior and Design for Externally Post-Tensioned Bridges,"* External Prestressing in Bridges, ACI SP 120-12, Proceedings of International Symposium, ACI, Detroit, Michigan, pp. 257-288.

[2] Aravinthan, T., Mutsuyoshi, H., Niitsu, T., and Chen, A. (1998). *"Flexural Behavior of Externally Prestressed Beams with Large Eccentricities,"* Proceedings of JCI, Vol.20, No.3, pp. 673-678.

[3] Aravinthan, T., Mutsuyoshi, H., Hamada, Y., and Watanabe, M. (1999). *"Experimental Investigation on The Flexural Behavior of Two Span Continuous Beams with Large Eccentricities,"* Proceedings of JCI, Vol.21, No.3, pp.961-966.

[4] Mutsuyoshi, H. (1997). *"New Technologies for Construction and Rehabilitation/ Strengthening of Bridges Utilizing External Prestressing,"* Concrete Journal, Vol.35, No.12, pp.3-11.

[5] Naaman, A.E. (1989). *"A New Methodology for the Analysis of Beams Prestressed with External or Unbonded Tendons,"* External Prestressing in Bridges, ACI SP 120-16, Proceedings of International Symposium, ACI, Detroit, Michigan, pp. 339-354.

[6] Naaman, A.E., and Alkhairi, F.M. (1991a). *"Stress at Ultimate in Unbonded Post-tensioned Tendons – Part 1: Proposed Methodology,"* ACI Structural Journal, Vol. 88, No. 5, pp. 641-649.

[7] Naaman, A.E., and Alkhairi, F.M. (1991b). *"Stress at Ultimate in Unbonded Post-tensioned Tendons – Part 2: Proposed Methodology,"* ACI Structural Journal, Vol. 88, No. 6, pp. 683-692.

[8] Vega, M., and Dotreppe, J.C. (1988). *"Numerical Procedure for the Analysis of the Ultimate Limit State Behavior of Prestressed Concrete Structures,"* Proceedings of FIP Symposium, Israel.

[9] Virlogeux, M.P. (1988). *"Non-linear Analysis of Externally Prestressed Structures,"* Proceedings of FIP Symposium, Israel.

[10] Alkhairi, F.M., and Naaman, A.E. (1993). *"Analysis of Beams Prestressed with Unbonded Internal and External Tendons,"* Journal of Structural Engineering, ASCE, 104(7), 119(9), pp. 2680-2700.

[11] Matupayont, S. (1995). *"Flexural Behavior of Externally Prestressed Concrete Beams,"* Ph.D. dissertation, Saitama University, Saitama, Japan.

[12] Matupayont, S., Mutsuyoshi, H., and Machida, A. (1994). *"Loss of Tendon's Eccentricity in Externally Prestressed Concrete Beam,"* Transaction of JCI, Vol. 16, pp. 403-410.

[13] MacGregor, R.J.G., Kreger, M.E., and Breen, J.E. (1989). *"Strength and Ductility of a Three-span Externally Box Girder Bridge Model,"* External Prestressing in Bridges, ACI SP 120-15, Proceedings of International Symposium, ACI, Detroit, Michigan, pp. 315-338.

[14] Lin, T.Y., and Thornton, K. (1972). *"Secondary Moments and Moment Redistribution in Continuous Prestressed Concrete Beams,"* Journal of PCI, Vol. 17, No. 1, pp. 1-20.

[15] Kordina, K., Hegger., J., and Teutsch., M. (1989). *"Shear Strength of Prestressed Concrete Beams with Unbonded Tendons,"* ACI Structural Journal, Vol. 85, No. 2, Mar.-Apr., pp. 143-149.

[16] Ito, T., Yamaguchi, T., and Ikeda, S. (1995). *"Flexural Shear Behavior of Precast Segmental Beams Prestressed with External Cables,"* Proceedings of JCI, Vol. 17, No. 2, pp. 773-778.

[17] Tan, K.H., and Ng, C.H. (1998). *"Effect of Shear in Externally Prestressed Beams,"* ACI Structural Journal, Vol. 95, No. 2, March-April, pp. 116-128.

[18] Guide to Good Practice (1978). *"Recommendations for segmental construction in prestressed concrete,"* Federation Euro-International de la Precontrainte (FIP), Wexham Springs, Slough, England.

[19] Mathivat, J. (1983). *"The Cantilever Construction of Prestressed Concrete Bridges,"* John Wiley and sons, New York, N.Y.

[20] ACI Committee 318. (1995). *"Building Code Requirement for Reinforced Concrete (ACI 318-95),"* ACI, Detroit, Michigan.

[21] Aravinthan, T. (1999). *"Flexural Behavior and Design Methodology of Externally Prestressed Concrete Beams,"* Ph.D. dissertation, Saitama University, Saitama, Japan.

[22] Menegotto, M., and Pinto, P.E. (1973). *"Method of Analysis for Cyclically Loaded Reinforced Concrete Plane Frames,"* IASBE Preliminary Report for Symposium on Resistance and Ultimate Deformability of Structures acted on well-defined repeated Loads, Lisbon, pp. 15-22.

[23] Lin, T. Y., and Burns, N.H. (1982). *"Design of Prestressed Concrete Structures,"* 3rd Edition, John Wiley & Sons, New York.

[24] Muller, J., and Gauthier, Y. (1989). *"Ultimate Behavior of Precast Segmental Box Girders with External Tendons,"* External Prestressing in Bridges, ACI SP 120-17, P, pp.355-373.

[25] Japan Society of Civil Engineers (JSCE). *"Standard Specification for Design and construction of Concrete Structures—Part 1[Design] (1986),"* 1986.

# APPENDIX : PHOTOGRAPHS OF EXPERIMENTAL WORK

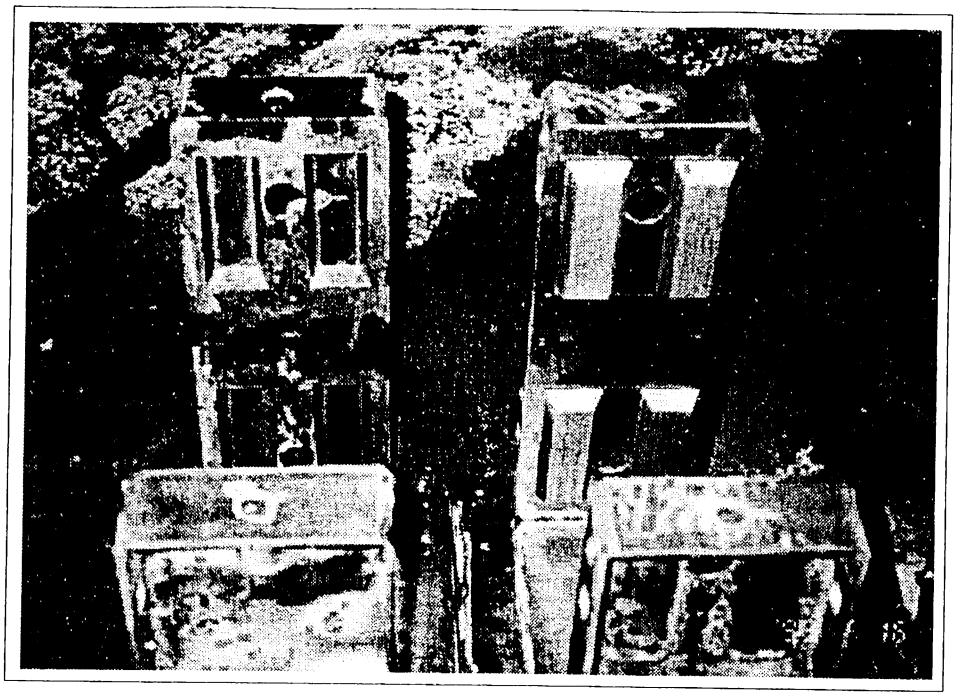

**Photo 1** Steel plate formwork with multiple shear keys

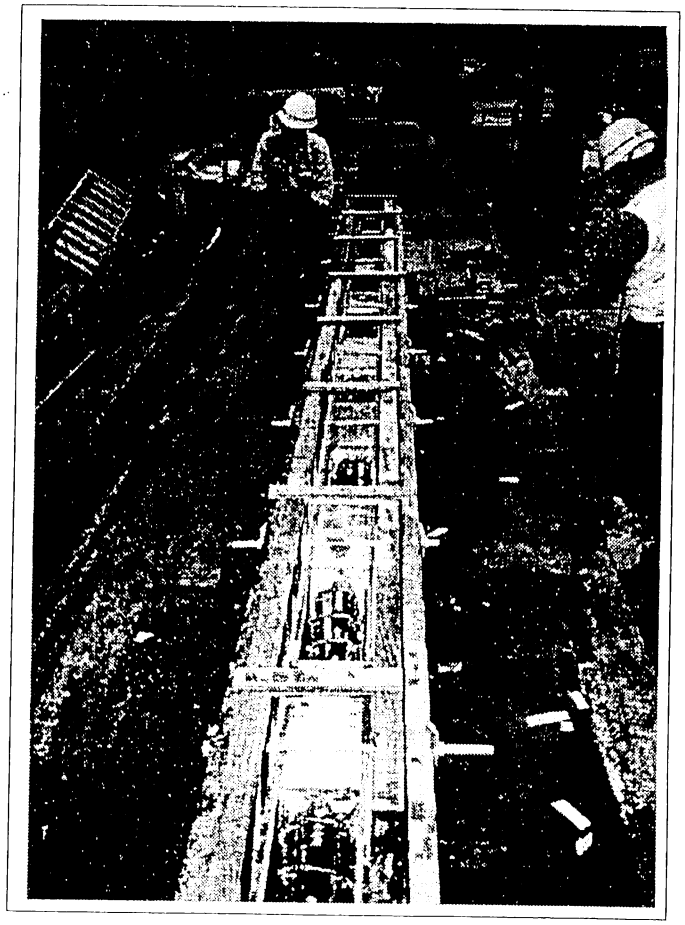

**Photo 2** Long-line match casting method (second casting)

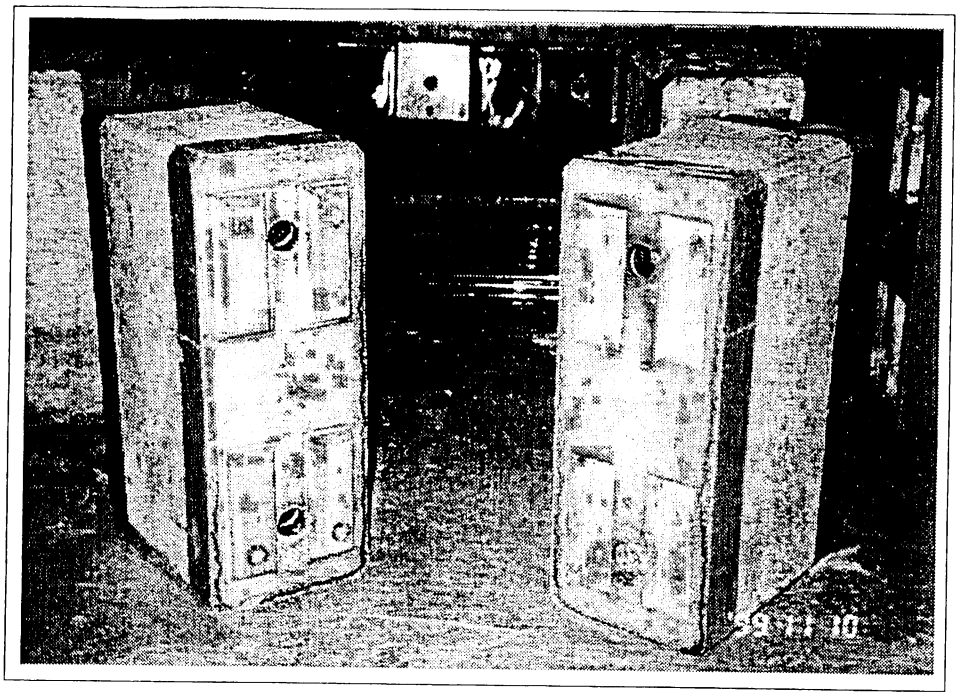

**Photo 3** Precast segments with male and female shear keys

**Photo 4** Preparation before assembly of precast segments

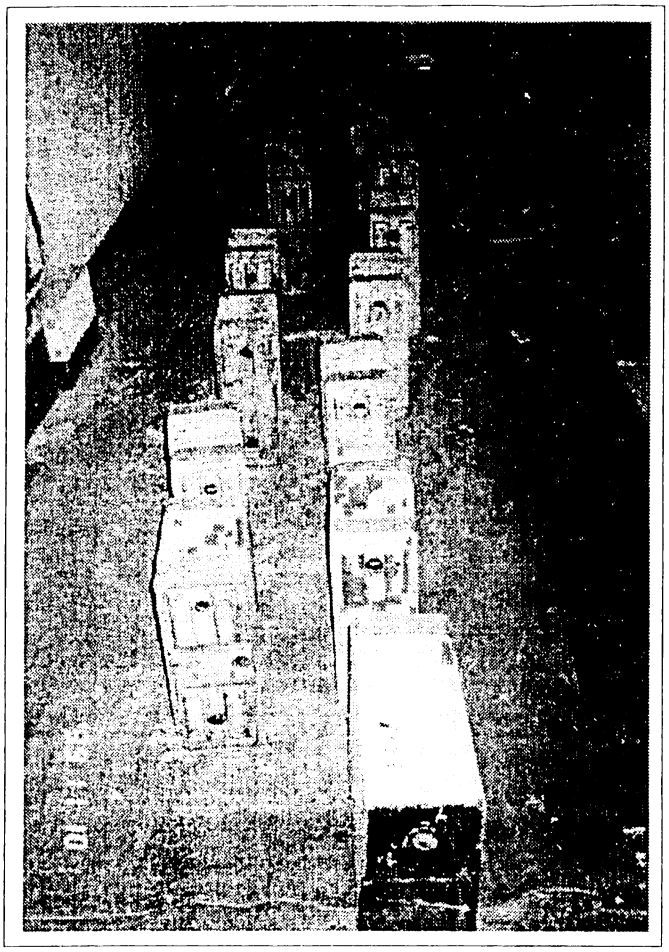

**Photo 5** Arrangement of precast segments before applying epoxy and initial prestressing

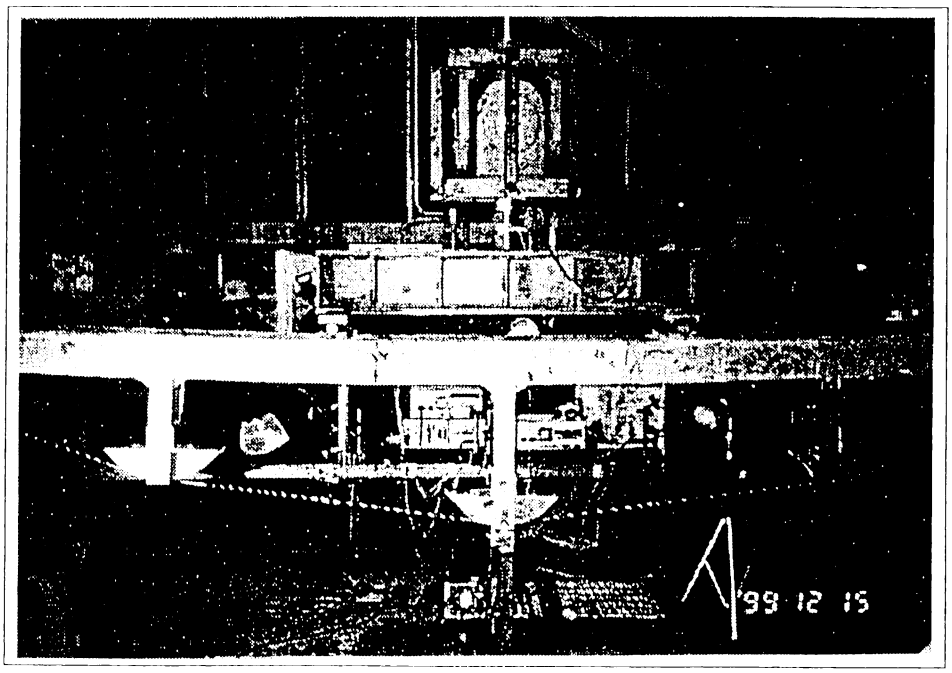


**Photo 6** Layout of test of single span beam D-1a (flexure-type)

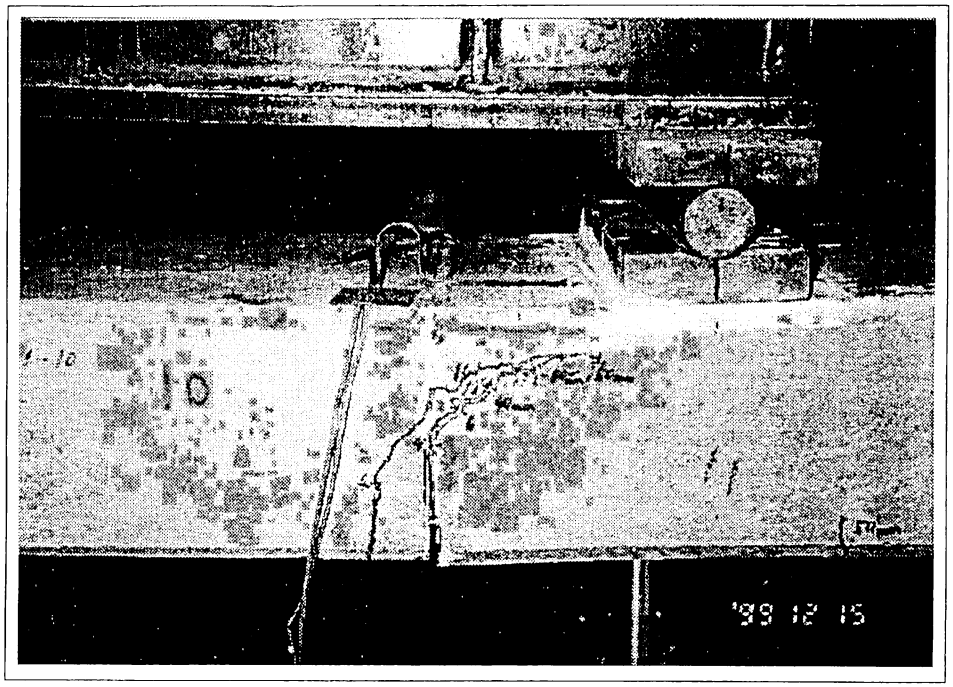


**Photo 7** Large opened joint and crack at ultimate load of beam D-1a

**Photo 8** Assembly of two-span continuous beam A-1a (flexure-type)

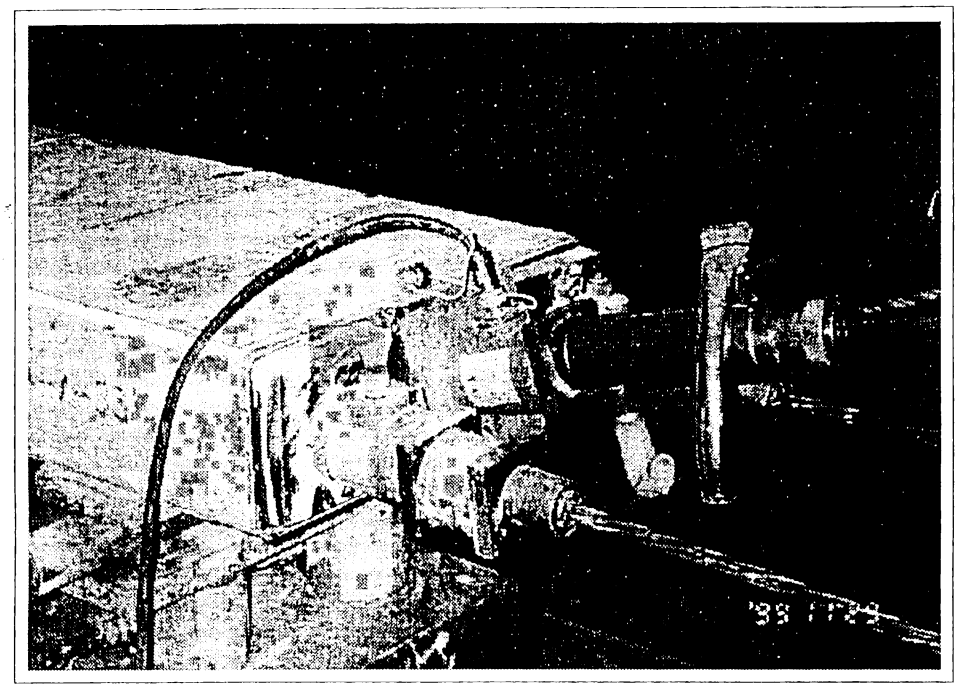

**Photo 9** Anchorage details with steel tube filled with epoxy for external tendon

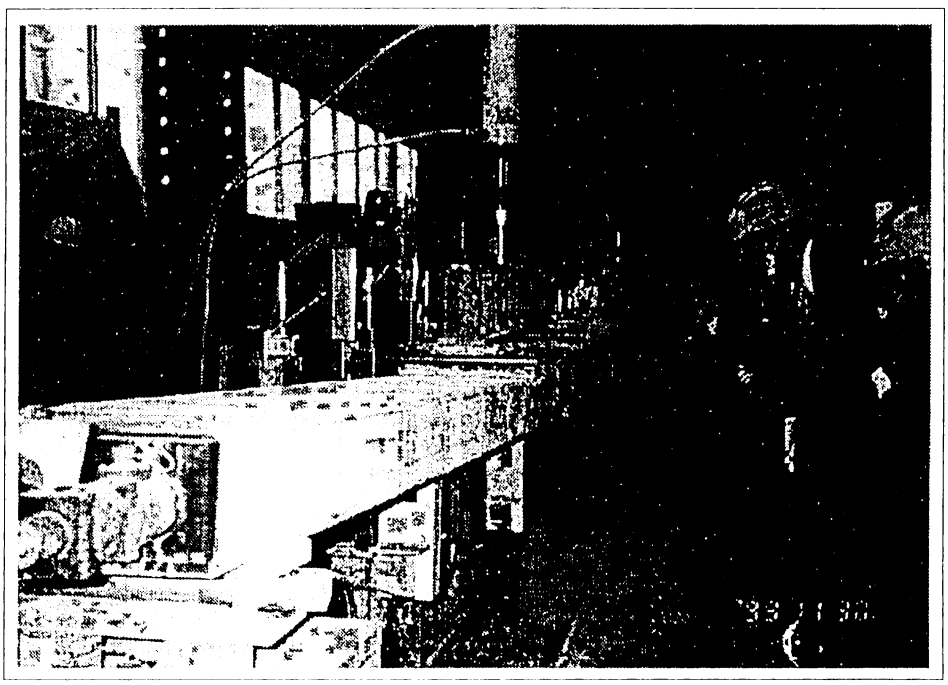

**Photo 10** Deformation shape of two-span continuous beam A-1a under loading

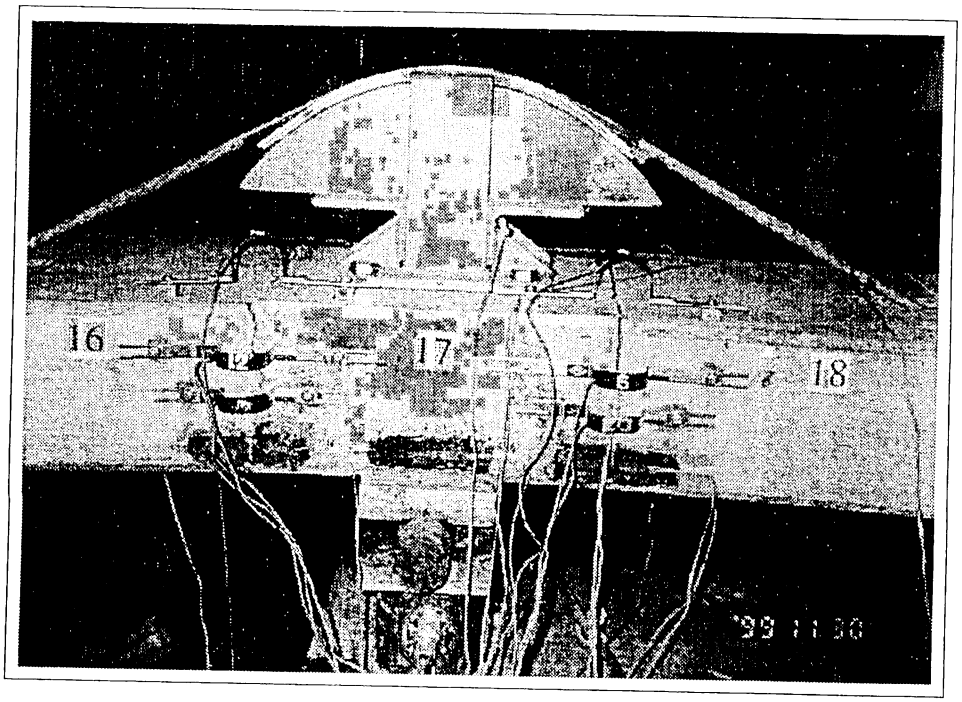


**Photo 11** Joint openings near center support region of beam A-1a

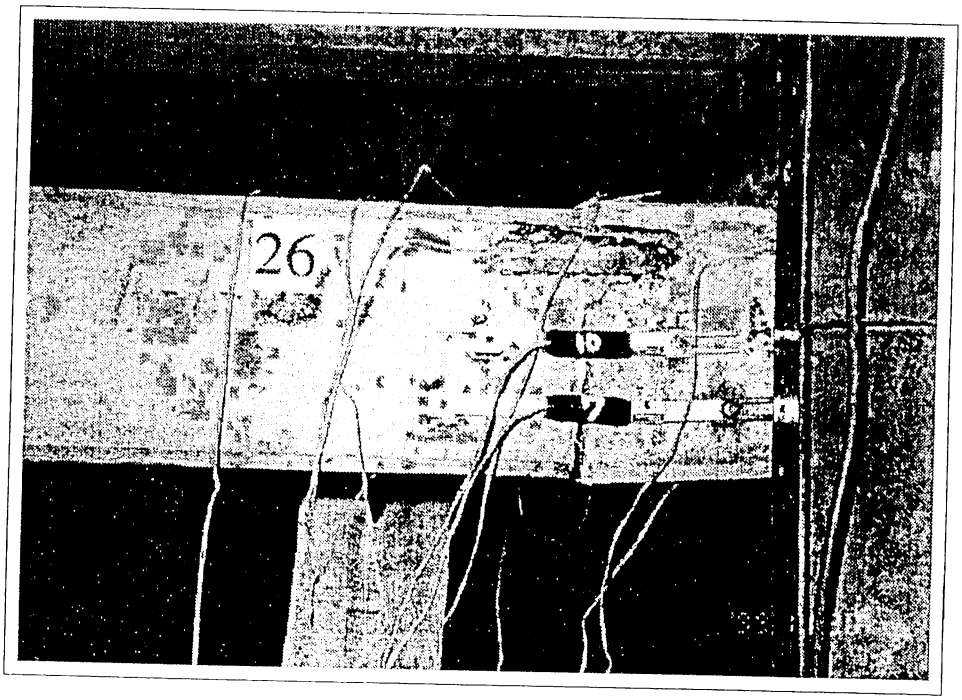


**Photo 12** Critical opened joint and crack near left loading point region of beam A-1a

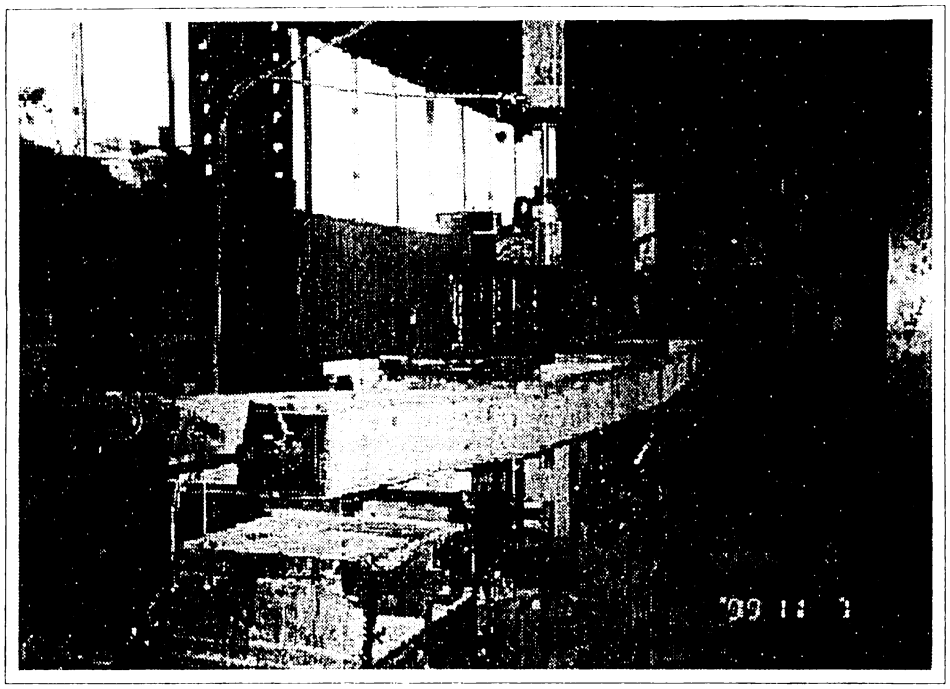

**Photo 13** Layout of test of shear-type specimens (S-type)

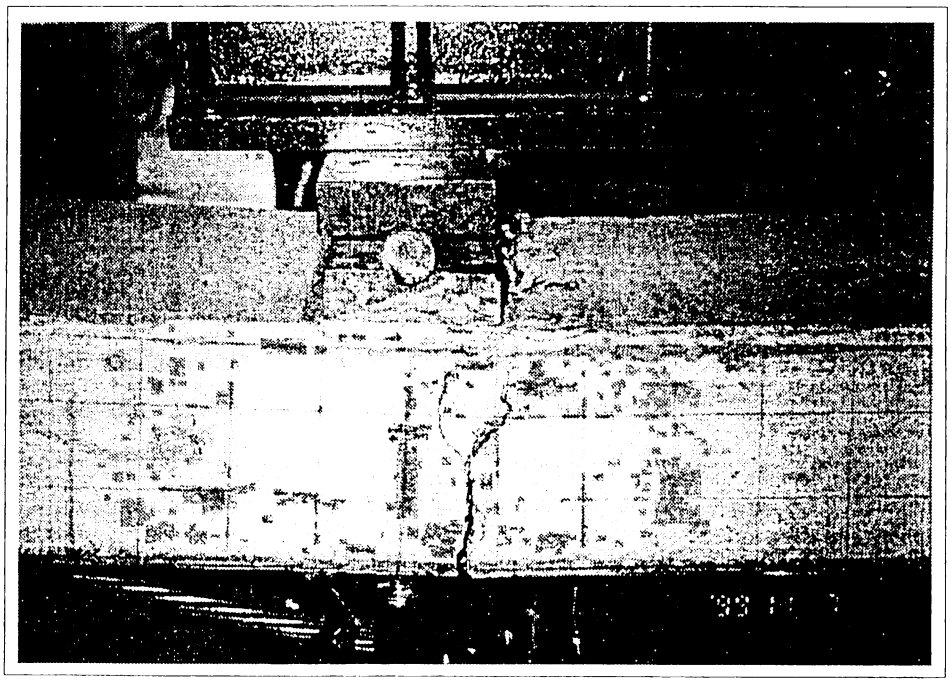

**Photo 14** Single large crack at ultimate load of monolithic beam S-1

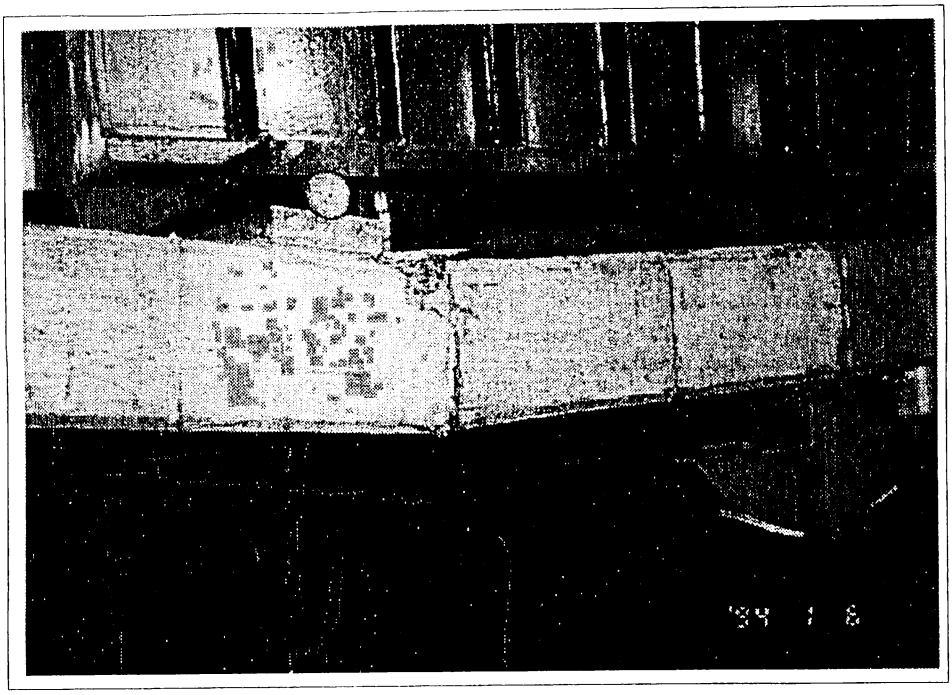

**Photo 15** Crushing of concrete and large joint opening of beam S-6 (smaller eccentricity)

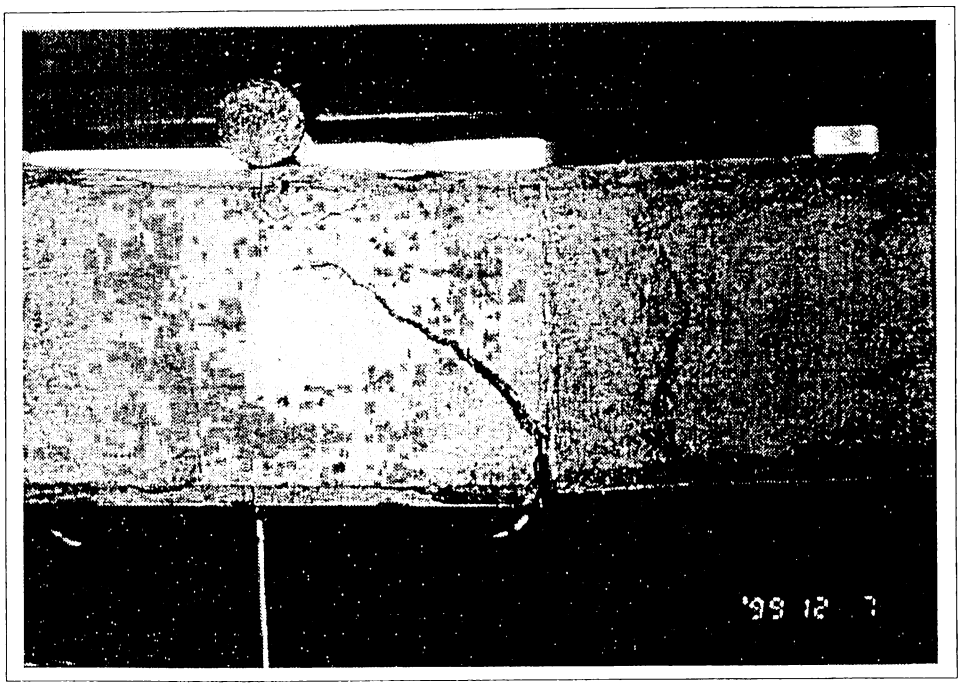

**Photo 16** Inclined crack at ultimate failure of beam tested without loading steel plates (beam S-3)

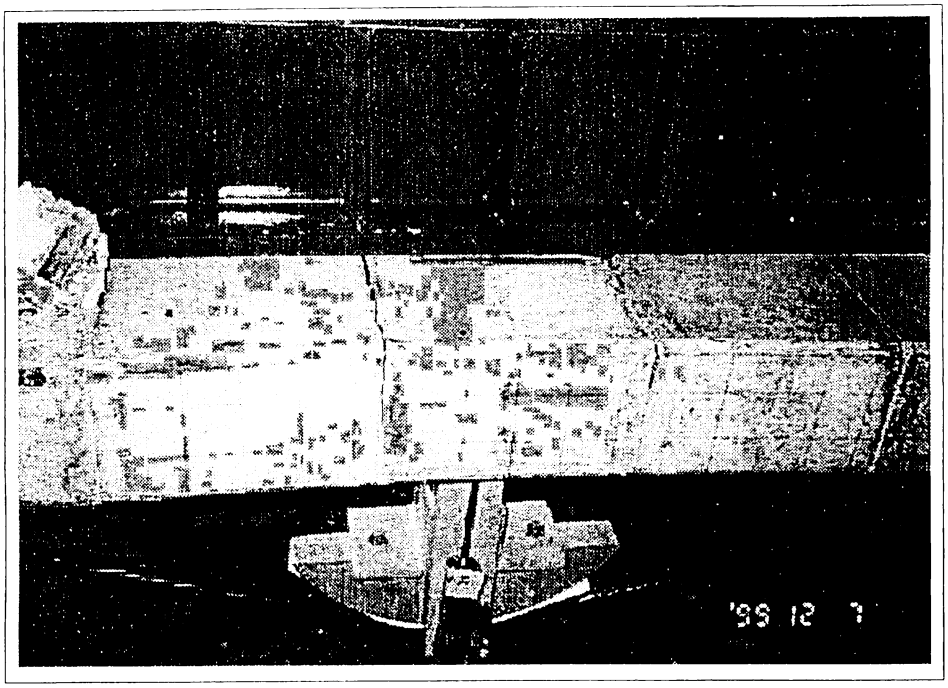


**Photo 17** Cracks at joints in mid-span region at the ultimate load (beam S-3)

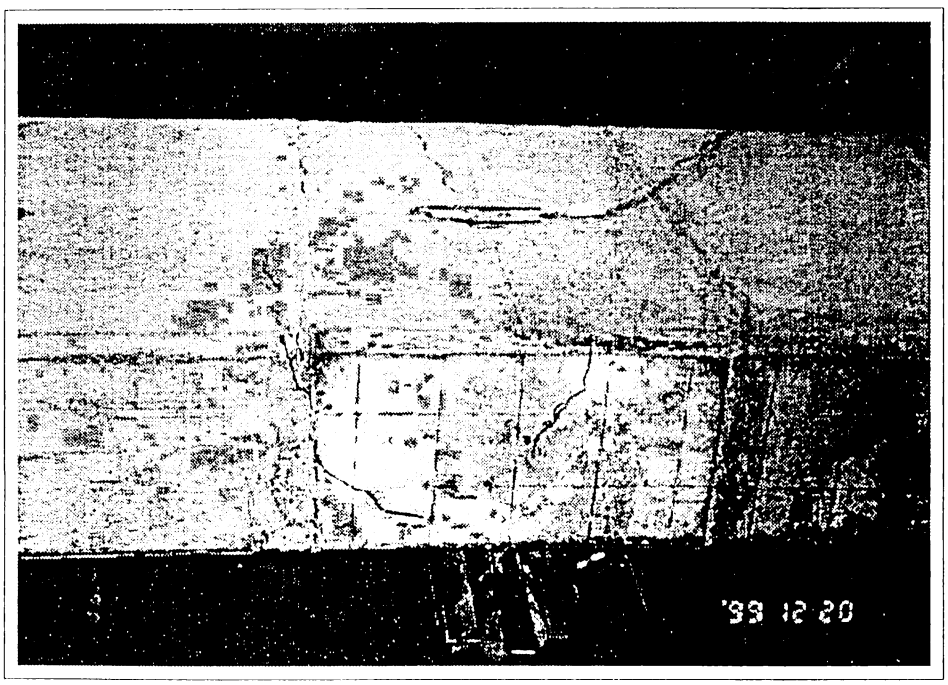


**Photo 18** Crack at end support at the ultimate load (beam S-4)